ADDIS ABABA UNIVERSITY

INSTITUTE OF TECHNOLOGY

SCHOOL OF CIVIL AND ENVIRONMENTAL ENGINEERING

GEOID QUASI-GEOID SEPARATION COMPUTATION USING THE GRACE AND GOCE GLOBAL GEOPOTENTIAL MODEL IN SEMIEN MOUNTAINS,ETHIOPIA

A thesis submitted to the school of graduate studies of addis ababa university in partial fulfillment of the requirements for the degree of masters of science in geodesy and geomatics (specialization in geodesy)

BY: TADEGE GETIE YISMAW

ADVISOR: TULU BESHA (Ph.D.)

August 2023

ADDIS ABABA

APPROVAL SHEET

Addis Ababa University

Institute of Technology (AAIT)

School of Civil and Environmental Engineering

Geodesy and Geomatics

This undersigned here by certify that have read and recommend to Addis Ababa university institute of technology school of civil and environmental engineering for ecceptance a thesis entitled "Geoid Quasi-Geoid Separation computation using the GRACE and GOCE Global Geopotential Model in Semien Mountains,Ethiopia"by Tadege Getie partial fulfillment of the requirements for the degree of masters of science in Geodesy and Geomatics (specialization in Geodesy)

Tadege getie

Tulu Bedke		17/07/2023
Advisor	**Signature**	**Date**
Sintayehu A		15/07/2023
Internal Examiner	**Signature**	**Date**
Ephrem Yaleu		15/07/2023
External Examiner	**Signature**	**Date**

Abrham Seble (Dr.)
Dean, School of Civil & Environmental Engineering

Chair Person	**Signature**	**Date**

Acknowledgments

In the first place, to God, the creator of the universe, who gave us the world so that we may learn about it and develop our minds, and to his mother, the Holy Virgin Mary, who is the reason for healing in the world? May the coronavirus cause the end of the world in a heartbeat, and may my thanks go to the Highest God, who gave me the insight and knowledge necessary to compose my dissertation. Secondly, I would like to thank Dr. Tulu Basha, who willingly accepted and arranged for me to consult on a research paper when you was assigned as a consultant at a time when he was struggling with national affairs.

Words cannot adequately describe my gratitude to Dr. Andinet Ashagra, who kept me entertained from beginning to end without once letting me get bored. I want to extend my profound gratitude to the brothers Sintayehu Abe, Nathaniel Agenagnew, and Gedamu ,Shumet Mengesha who have consistently served as my inspiration and motivators.Last but not least, I extend my sincere gratitude to my family, whom I adore and respect beyond all else.

Content

I

List of Figure

List of Table

List of Acronyms

A.A	Addis Ababa
ANRS	Amara National Regional State
CSR	Center for Space Research
CSRC	Center for Space Research
DEOS	Delft Institute of Earth Observation and Space Systems
DFACS	Drag-Free and Attitude Control System
DLR	Germany Euro Space Center
DTM	Digital Topographic Model
ECMWF	European Center for Medium-range Weather Forecasts
EGM	Earth gravitational model
ESA	Earth Explorer Program
GFZ	GeoForschungs Zentrum
GIS	Geography information system
GNSS	Global navigation satellite system
GOCE	Steady-State Ocean Circulation Explorer
G GRGS	Groupe de Recherché de Geodesies Spatial
GRACE	Gravity Recovery and Climate Experiment
ISDC	Integrated System Data Center
JPL Jet	Propulsion Laboratory
KBR	K-band ranging
KSDC	Science Data Center
LORF	Local Orbital Reference Frame
LRR	laser retroreflector
NASA	National Aeronautics and Space Administration
NCEP	National Centers for Environmental Prediction
POD	Precise orbit determination
PODAAC	Physical Oceanography Distributive Active Data Center
RMS	root mean square
SGG	Satellite Gravity Gradiometry
SMNP	Simien mountain National Park
SST	Satellite-to-Satellite Tracking
USA	United States of America

Abstract

Different reference systems are used to determine height,which are quasi-geoids and geoids. The definition of the geoid and telluroid (or, more generally, the quasi-geoid) is connected to these height systems. The optimal technique for computing orthometric heights has been a topic of discussion for more than a century. In mountainous regions, it is challenging to determine geoid and quasi-geoid features using GPS technology. The highest point of a mountain in Ethiopia's highlands is known as Ras Dashen. To tackle boundary issues for mountainous places such as the Ethiopian Semein plateau, a satellite data model is required to ascertain the distinction between geoid and quasi-geoid. We have written this research article to support this investigation. For individuals working in this field, determining the distance between the two references is quite helpful. Calculating the distance between them is important to transform what we receive from one to another.Although there are other ways to determine this gap, we employed satellite earth models created using satellite data for this work. There are three different kinds of models: models created only using GRACE satellite data, models created only using GOCE satellite data, and models created using both GRACE and GOCE data. Our search for the model reference height type was based on E Topo. As a result, Sjoberg's exact formula was used to calculate it in this study using the geoid-quasi-geoid separation model. Using the ETOPO 1 and TC programs from the GRAVSOFT package, the gravity anomaly in the case area was determined. This study investigated variations in the results of the order factor in the application of gravity in addition to the type of data. Models from the International Center for Global Earth Models, including SGG-UGM-2, IGGT_R1C, GO_CONS_GCF_2_TIM_R6, and ITSG-Grace2018, were used in this determination of Geoid-Qusigeoid separation.With the help of these models, we searched for various gravitational field functions, but primarily we searched for the separation between the geoid and quasi-geoid separation in all four models, and we discovered that the minimum and maximum results are, respectively, 0.388, 0.356, 0.365, 0.360 and 4.730,3.798,3.755,and 3.760 meter.

***Key words**: Geoid, height anomaly, gravity anomaly, quasi-geoid, height undulation, quasi-geoid separation*

CHAPTER ONE

1 Introduction

1.1 Background of the study

Determining the geoid, which is an equipotential surface of the Earth's gravity field that generally coincides with mean sea level, is one of geodesy's most important tasks. The geoid surface is significantly smoother than the actual surface of the Earth, but it is more irregular than the ellipsoid of a revolution, which is frequently used as an approximation of the shape of the physical Earth. The orthometric and normal heights are the most widely used concepts for the creation of vertical reference frames globally. These concepts are derived from the reference of the geoid and ellipsoid. These height systems are connected to how the geoid and telluroid (or more generally, the quasi-geoid) are defined. It has been discussed for more than a decade how to evaluate orthometric heights.(Bagherbandi & Tenzer, 2013)

The geodetic community has decided to use the Earth's gravitational field as the orthometric height system's reference surface because it best fits Mean Sea Level (MSL) (in the least squares sense)(Mehramuz & Zomorrodian, 2013). Moreover, Helmet is also credited with the first theoretical effort. The Poincare-Prey gravity gradient is utilized in Helmert's definition of the orthometric height to determine an approximation of the mean gravity of gravity measured at the surface location. On the other hand, Molodensky defined the mathematical surface that serves as a reference for the normal height (Bagherbandi & Tenzer, 2013).

According to the reference, the telluroid is a mathematical surface where the normal potential of points is identical to the actual potential of corresponding points on the earth's surface. Molodensky described the telluroid as such. Methods of evaluating the height anomalies have since been addressed, for example by Hörmander and Holota, with references to the formulation of the Molodensky boundary-value problem. The geoid-to-quasi-geoid adjustment is typically approximated in the geodetic literature by the difference between Helmert's orthometric and Molodensky normal heights. This approximation states that the correction depends on the planar simple Bouguer gravity anomaly. However, when evaluating the real values of the geoid-to-quasi-geoid adjustment, this approximation could result in a centimeter or even decimeter mistake.(Tenzer, Moo,r e et al., 2006)

The limitations of the geoid and quasi-geoid models prevent many nations from using GNSS-leveling, which is the method of leveling by GNSS plus a gravimetric geoid model. Future

advancements in GNSS technology for precise positioning may be anticipated, which will raise the demand for even more precise geoid models. Parallel to this, the precision and density of the global and regional gravity field data will be significantly higher, which will be extremely helpful for accurate geoid and quasi-geoid modeling. This is especially true if such development is accompanied by the essential advancements in geoid computing techniques, which include full corrections for all kinds of mistakes and the best possible combination of multiple data sources. (Sjöberg, 2018)

The major objective of the current study is to demonstrate the distinction between geoid to quasi-geoid separation in the Semain plateau using the Gravity Recovery and Climate Experiment and the Gravity Field and Steady-State Ocean Circulation Explorer.

1.2 **Statement of the problem**

One of the geodesists' active research areas is the precise estimation of orthometric heights (Schubert et al., 2001). In order to calculate orthometric heights from geopotential heights, it is necessary to approximate the gravity fluctuation along the plumb line from the surface to the geoid(Tenzer, et al., 2006). Instead of requiring knowledge of the real gravitational pull at measurement places, Normal Heights are simpler to calculate.But height system can be chosen based on personal preference and may be influenced by the cost of data generation(Molnar et al., 2015). The topographic surface of the Earth is complicated and uneven compared to the geometrically simpler shape of a perfect spheroid. It is difficult to map a flat surface to the earth's surface. (Seid, 2019)

Typically, the difference between Helmert's orthometric and Molodensky's normal heights is used to estimate the geoid-to-quasi-geoid adjustment. This approximation states that the correction depends on the planar simple Bouguer gravity anomaly(Tassis et al., 2013). However, the determination of the true value of the geoid-to-quasi-geoid correction can result in centimeter- or even decimeter-sized errors due to this approximation(Sjo, 2000). This means that a more precise formula must be used in the computation in order to attain high precision, especially in mountainous areas. A more precise definition of the geoid-to-quasi-geoid correction is created by contrasting the geoidal height and height anomaly, together with key characteristics of numerical realization(Tenzer,et al., 2006).

Historically, the planar Bouguer gravity anomaly and topographic height have been used to calculate the geoid-to-quasi-geoid adjustment. The computation of this correction using the approximate approach, however, produces considerable inaccuracies, particularly in

mountainous locations with computation points at high elevations, according to current numerical studies based on newly created theoretical models.(Bagherbandi et al., 2013)

Understanding the distinction between a geoid and a quasi-geoid makes it simpler to translate measurements between orthometric height and normal height(Sjöberg, 2018). The quasi-geoid is increasingly being used as a reference today. For engineering purposes, it is crucial to convert this measurement to orthometric height(Hofmann, et al., 2017). Understanding the distinction between the geoid and the quasi-geoid would be helpful in this at locations where ground surveys cannot be conducted at extremely high places, this work can be accomplished by using a satellite data model(Jekeli et al., 2009). The study started, thinking that it was crucial to do so, to assist in completing these chores. Based on the assumption that this issue exists, this study is based on Ethiopia's Semien plateau.The northern mountain was constructed with the idea that by comprehending the variations in this mountain, one will be able to comprehend the vast variations in the nation because it is the first of the country's highest points. The Semian plateau, which is the highest peak point in Ethiopia and the fourth level in all of Africa, this study will look into the approximate separation between geoid and quasi-geoid in this place.

1.2 Objectives of the Study

1.2.1 General Objective

The main objective of this study is to determine geoid to quasi-geoid separation in Semian plateau from Gravity Recovery and Climate Experiment and the Gravity Field and Steady-State Ocean Circulation Explorer satellite data model.

1.2.2 Specific objective

This research has the following specific objectives:

- To Comparing different gravity field functions in the study area using GRACE and GOCE satellite data models.
- To determine the geoid to quasi-geoid separation of the study area using the GRACE and GOCE satellite in higher order data models.
- To investigate the effects of the number of degrees and orders of earth model data in the gravity field function calculation and geoid to quasi-geoid separation.

1.3 Significance of the Study

The results of the current study will include details on the precise determination of geoid-to-quasi-geoid separation on the mountain as well as details on several geoid-to-quasi-geoid separation models and the importance of each for precisely determining height. The current study can serve as a starting point for future local-level evaluations of geoid in quasi-geoid separation and related domains throughout Ethiopia.

1.4 The scope of the study

Semien plateau,(Ras Dejen Mountain), which is a part of Semien Mountain National Park, is where this study would be conducted in the Amara region. Different topographies exist in the research area. The task of establishing the geoid to the quasi-geoid separation of mountains is exceedingly challenging and laborious for geodesists due to the extremely rough texture of the earth's surface. For various applications, particularly geodesy applications, the precise measurement of geoid and quasi-geoid separation is required. The geoid-to-quasi-geoid separation of the earth has been calculated using various techniques by scientists. This is the transition between old-fashioned spirit leveling and current GNSS technology based on satellites. To determine the quasi-geoid separation, the geoid must meet certain physical criteria. Since GRACE and GOCE satellite data models can be used to calculate the geoid to quasi-geoid separation, this study is focused on doing so.

1.5 Structure of study

Six major chapters comprise the structure of the current study. The study context, introduction, problem statement, study objective (both general and specific objectives), significance, and scope are all covered, in the first chapter of the study. In the second chapter, the literature review is covered. This chapter introduces some works pertinent to the topic of the current study, Geoid-Quasi Geoid Separation Computation Using Gravity Recovery and Climate Experiment and the Gravity Field and Steady-State Ocean Circulation Explorer satellite data model. The third chapter provides a general overview of the study field, along with information on the data sources, data processing, and general methodological flowcharts. Including its location, climate, and topography, the research region is thoroughly described in this chapter. In the fourth chapter, the findings and analysis are given. The fifth chapter discusses the study, while the final chapter six includes recommendations and conclusions.

CHAPTER TWO

2. Literature Review

2.1 Geoid

The surface of constant potential energy known as the geoid is located where the mean ocean surface elevation corresponds with the earth's surface. Potential energy which in this context refers to both gravitational and centrifugal potential energy is used. This is how the geoid is typically defined, although it's a poor definition. One reason is that dynamic processes occurring within the ocean prevent the mean sea level from being completely a surface of constant potential. Although it is possible to envision turning off dynamic processes so that the sea level remains a potential constant surface(Gedamu et al., 2020).

A constant potential surface makes up the surface of an equilibrium fluid, as we'll demonstrate later. Additionally, the geoid lies underneath the earth's surface wherever there are continents. As a result, the gravitational attraction of the underlying mass warps the actual equal potential surface beneath the continents. However, geodesists describe the geoid as if those masses were below it rather than above it. Their geoid is not actually an equipotential surface, to put it another way. (Vaníček, 1976)

In surveying practice, it is widely accepted that heights of practical value must be expressed as mean sea level; Vanicek was one of many authors to explain why in 1998. Therefore, it is necessary to know the mean sea level beneath the continent in order to acquire some heights of practical value. Such heights have been proved to be advantageous in the majority of engineering applications and are intuitively appealing. (Kingdon et al., 2012)

A gravity equipotential surface with a constant gravity potential W roughly follows where the mean sea level is. Additionally, the surveying equipment is positioned so that it is perpendicular to the gravity equipotential surfaces and aligned with the local gravity vector, which makes the gravity field a crucial factor in practical height calculation.(Shandini & Tadjou, 2012)

The horizontal (level) surface that passes through the equipotential surface of the Earth's field at point a. There is only one such surface that passes through every point, as shown in Fig. 1, and it is the surface on which every homogeneous fluid will stable on the left alone. Seawater does not actually follow a horizontal surface because it is not uniform due to variations in temperature, composition, etc. at different locations. Horizontal currents, some of them fairly strong, result from this. But since the sea surface is quite close to an equipotential surface, within a tolerance of plus or minus 2 meters, we can logically use an equipotential surface as

the reference surface for heights. One of the focuses of this work is the determination of such a horizontal surface, known as the geoid, which most closely resembles mean sea level. (Kingdon et al., 2012)

The Stokes formula (Stokes 1849), used in gravimetric geoid modeling, integrates the gravity anomaly on a sphere that approximates the surface of the Earth to get the geoid height, or the height of the geoid above the reference ellipsoid. Modern methods modify Stokes' formula in a number of ways, most notably by taking into account an Earth Gravitational Model (EGM) to represent the long wavelengths of the geoid while, essentially, only short wavelengths are governed by surface gravity. (Ågren et al., 2008)

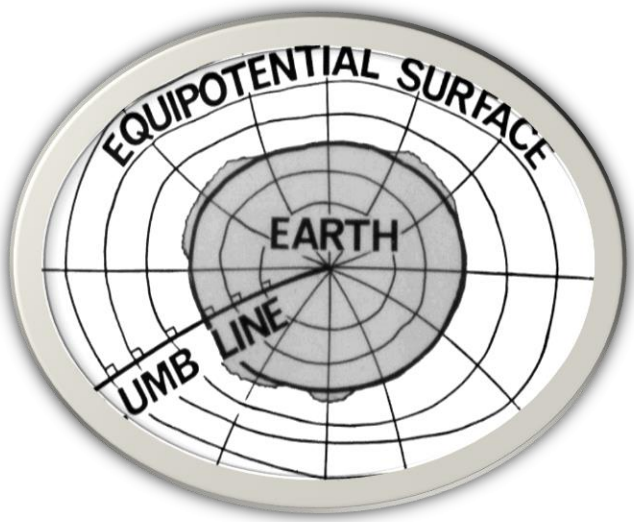

Figure 2.1 Structure of Earth's gravity field

The primary determined surface gravity anomaly data must undergo various modifications before applying Stokes' formula. The data must be: a) Corrected for the topographic effect on gravity anomaly (direct topographic effect on gravity anomaly), b) Corrected for the atmospheric effect (direct atmospheric effect), and c) Reduced from the Earth's surface to the sphere (downward continuation, downward continue the effect) because the formula is performed on a sphere and does not allow masses external to the sphere. (Sjöberg, 2010)

2.2 The Ellipsoid

For the real earth, the ellipsoid is a better approximation of the geoid than, say, a sphere. We'll refer to the distinction between the geoid and the ellipsoid later on when we discuss geoid heights for the actual earth. (Tenzer et al., 2006)

Molodenski declared the geoid to be impossible to determine with sufficient accuracy and introduced an alternative quantity known as the quasi-geoid due to the fact that the top density

was not known with acceptable accuracy back in the 1960s and that this difficulty still exists today. Since then, several mathematical and theoretical advancements have improved the methods of Molodenski et al for determining the quasi-geoid, particularly the formulation in terms of analytical continuation as detailed .(Mccubbine et al., 2018)

Fig. 2.2 depicts how the quasi-geoid interacts with the geoid, the geoid, and the reference ellipsoid. The quasi-geoidal height, also known as the height anomaly, is the vertical separation between the quasi-geoid and the reference ellipsoid. Since all calculations are performed on the Earth's surface (or a surface that is almost equal to it, called the telluroid) and not on the geoid, it would not be essential to know the topo-density in order to determine the quasi-geoid. (Kingdon et al., 2012)

The entire time, Molodenski's hypothesis focuses on the Earth's gravitational potential outside of its surface. Since Molodenski's method only interacts with the external field and only needs to be familiar with the external field's geometry, it does not require any knowledge of the top density. However, because the method is based on geometry, it necessitates integration over the Earth's surface, to be more precise. (Kingdon et al., 2012)

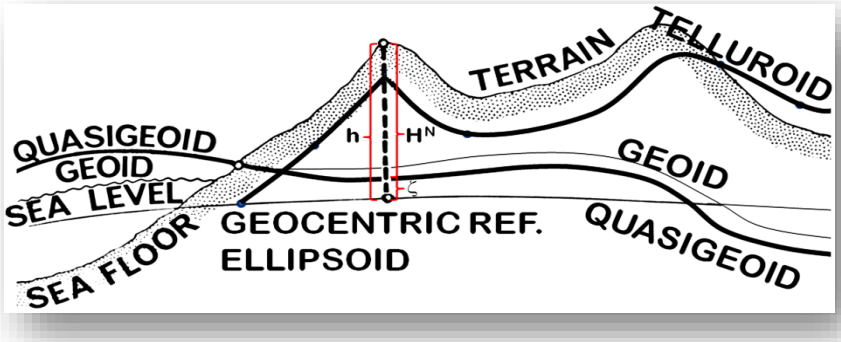

`

Figure 2.2. The relation between the quasi-geoid, geoid, and reference ellipsoid

2.3 Type of Height systems

The vertical distance of points from the origin surface, which has zero height, must be stated in order to calculate the heights of earth points. A variety of surfaces can be used as a guide for heights. The geoid is the most crucial surface out of these. Different physical and geometrical meanings apply to reference surfaces and the vertical distances of points from the surface. Geodetic heights also have several geometric and physical meanings. As a result, researchers introduced a number of height systems, some of which were investigated in the following manner.(Sadiq et al., 2009)

2.3.1 Orthometric heights

The standard "practical height" above sea level used in engineering and mapping is H. There are other, less common heights that pertain to sea level, and we'll look at one of them in the following section the usual height. The plumb line, which is always tangent to the gravity vector and extends from the geoid to the point of interest, is used to calculate the orthometric height of each point of interest. (Hofmann et al., 2017)

The most physiologically significant heights, known as dynamic heights, will not be discussed in this article because they are rarely used in engineering, mapping, or practice. Other, less frequent heights apply to engineering and sea charting. In the Americas, as well as in parts of Africa and Asia, orthometric heights and geoidal heights are commonly utilized. Recently, it was decided that the US and Canada should use a geoidal model and orthometric heights as their national systems of heights. (Huang et al., 2013)

2.3.2 Geodetic heights

H are heights above the biaxial "geocentric reference ellipsoid," determined by measuring along the ellipsoid's normal. However, they are of very little practical value on their own and are easily ascertained from satellite observations. (Sjöberg, 2008)

However, as we can see in Fig. 3, if the geoid's deviation from the geocentric reference ellipsoid N is subtracted from a geodetic height h, we obtain the orthometric height H, which can then be applied in practice.

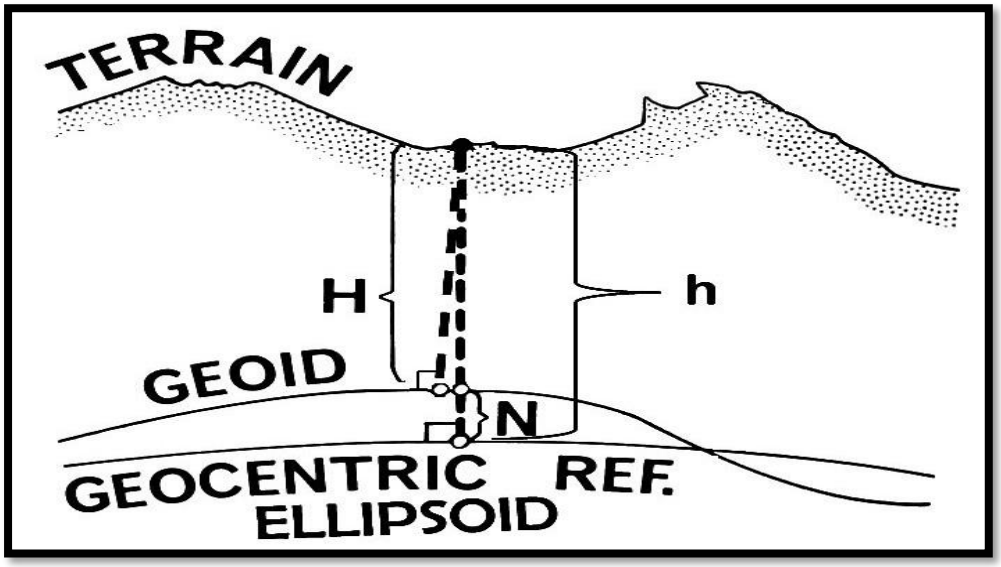

Figure 2.3. Relation between geoid, geodetic, and orthometric heights

Geoidal heights serve as a bridge between practical heights (orthometric) and geodetic heights, which are measured by satellite. (Hofmann et al., 2017)

Normal height is defined as the height measured above the ellipsoid and is used in the former Soviet Union and nine other European nations (France, Germany, Sweden, Poland, the Czech Republic, the Slovak Republic, Hungary, Romania, and Bulgaria). A point's normal height on the topographical surface is determined by measuring it along the normal plumb line from the corresponding point on the telluroid above the reference ellipsoid. Normal heights, when measured along the normal plumb line, can also be thought of as the heights of the topographical surface above the quasi-geoid.(Huang et al., 2013)

The geoid height topography model can also be converted into a surface spherical harmonics expansion in spherical harmonics (S Neeun, 1994 provides an excellent overview of this method).

$$H(\lambda,\varphi) = R(\sum_{l=0}^{l_{max}} \sum_{m=0}^{l} P_{lm}(sin\varphi)(C_{lm}^{topo} cosm\lambda + S_{lm}^{topo} sinm\lambda) \quad (1)$$

where the expansion's coefficients, C_{lm}^{topo} and S_{lm}^{T}, are typically scaled by the reference radius R. The geoid height N can be approximately calculated using the same expansion's upper limit, ℓ_{max}.(Al-Dabbagh, 2014)

2.4 The Gravity Field of the Earth

According to (Toth et al., 2008), the following is a thorough explanation of the importance of the earth's external gravity field in geodesy:

1. The vast majority of measured quantities in geodesy use the external gravity field as their reference system. To reduce the quantities to geometrically defined systems, this field must be understood.

2. If the distribution of gravity values on the earth's surface is known, other geodetic measurements can be used to establish this surface's shape.

3. The level surface of the gravity field, also known as the geoid, is the most crucial reference surface for height measurements.

4. Information on the composition and properties of the earth's interior can be gleaned through the analysis of the external gravity field. Geodesy is transformed into a geophysics auxiliary science by making the necessary gravity field parameters available. (Toth et al., 2008)

2.5 Potential and the Geoid

According to the theory of harmonic functions, understanding just one equipotential surface is enough to define a whole harmonic function outside of it. The geoid is one equipotential surface that is particularly significant for the Earth. The geoid is the equipotential surface

that, as shown in Fig. 2.4, coincides with the undisturbed sea surface and its hypothetical continuation beneath the continent.(Hofmann, etal.,2017)

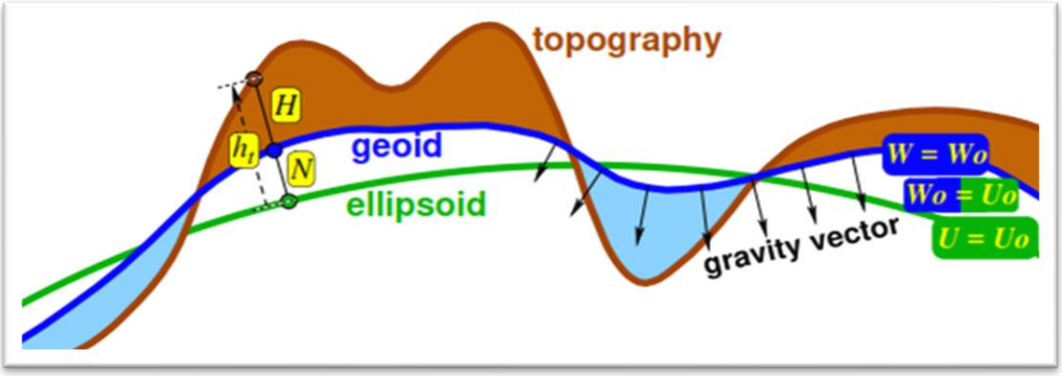

Figure 2.4. Ellipsoid, geoid, and topography

The geoid is a surface to which gravity always exerts a perpendicular force (but not one that is equal in strength!), since it is an equipotential surface.

(As per usual, we divide the potential W into the normal potential U and the disturbing potential T, and define "shape" and "strength" of the normal potential as follows: (a) The equipotential surface of the normal potential U for which U (x, y, z) = U0 holds should have the form of an ellipsoid of revolution, and (b) this equipotential surface should closely resemble the geoid, or the undisturbed sea surface, in the sense of least squares fit. (Xu et al., 2017)

It is useful to define the ellipsoidal coordinates (h, λ, φ) with respect to the ellipsoid U (h = 0) = U0 = W0, where h denotes the height above the ellipsoid (measured along the ellipsoidal normal), denotes the ellipsoidal longitude, and denotes the ellipsoidal latitude. As heights N to the ellipsoid (U = U0) as a function of the coordinates and, N (λ,ϕ) is the typical representation of the geoid. N is the undulation of the elliptical geoidal surface as a result. The Geodetic Reference System refers to this geometric ellipsoid and the typical ellipsoidal potential. (Moritz, 1992)

We now have two reference surfaces the ellipsoid and the geoid—to which the height of a point can be expressed. The height of the Earth's surface, or the height of the topography relative to the ellipsoid and the geoid, will be denoted by h_t and H, respectively, as shown in Figure 2(Kingdon et al., 2012)

Spherical harmonics, often known as Stokes' coefficients, are spectral representations of the global structure and irregularity of the geopotential field, or more generally, the Earth's gravitational field. The following equation describes how the geopotential's spectral and spatial domains are related:

$$W_a(r,\lambda,\varphi) = \frac{GM}{r}\sum_{l=0}^{l_{max}}\sum_{m=0}^{l}\left(\frac{R}{r}\right)^{l} p_{lm}(sin\varphi)(C_{lm}^{W}cosm\lambda + S_{lm}^{W}sinm\lambda) \quad (2)$$

This shows the 1/r-behavior for r → ∞, written in the form

$$W_a(r,\lambda,\varphi) = \frac{GM}{r}\sum_{l=0}^{l_{max}}\sum_{m=0}^{l}\left(\frac{R}{r}\right)^{l+1} p_{lm}(sin\varphi)(C_{lm}^{W}cosm\lambda + S_{lm}^{W}sinm\lambda \quad (3)$$

This is sometimes useful in practice. The notations are: -spherical geocentric coordinates of computation (radius, longitude, latitude). R reference radius, GM-product of gravitational constant and mass of the earth. L, m degree, order of spherical harmonics, P_{lm}-fully normalized Legendre function C_{lm}^{W}, S_{lm}^{W} Stokes coefficient (fully normalized).

The transformation formulas between ellipsoidal (h,λ,φ) and spherical(r,λ,φ)) coordinates can be found, e.g., in A spherical harmonic approximation of the gravity field up to a maximum degree l_{max}(a so-called "gravity field model") consists of (l_{max} + 1+1) ^2 coefficients and 2 values of GM and R to which the coefficient(Hofmann-Wellenhof et al., 2005).

2.5.1 The Height Anomaly

The height anomaly ζ(λ, ϕ), the well-known approximation of the geoid undulation according to Molodensky's theory, can be defined by the distance from the Earth's surface to the point where the normal potential U has the same value as the geopotential W at the Earth's surface (Hofmann-Wellenhof et al., 2005)

In spherical harmonics, the height anomaly approximates the geoid according to Molodensky's theory. It is equal to the geoid over the sea.

Here it will be calculated, as defined on the Earth's surface approximated by Burns' formula on the ellipsoid plus a first-order correction. The elevation information is automatically taken from the ETOPO1 topography model.

$$\zeta 1(\lambda,\phi) \approx \zeta e1(\lambda,\phi) + \left(\frac{h_t}{\gamma_0} * \frac{\partial T^c}{\partial h}|h = 0\right) \quad (4)$$

The calculation of the height anomalies ζ (ϕ, λ) from the spherical harmonic potential model according to iteration equation 4 is possible using. Without using a topography model, they can be calculated .

$$\zeta_{e1}(\lambda,\varphi) = \frac{GM}{r_e\gamma(r_{e,}\varphi)}\sum_{l=0}^{l_{max}}\left(\frac{R}{r_e}\right)^{l}\sum_{l=0}^{l} p_{lm}(sin\varphi)(C_{lm}^{T}\cos m\lambda + S_{lm}^{T}sinm\lambda$$

$$\zeta_1 = \left(\zeta_{e1} + \frac{H_{(\varphi,\lambda)}+(N_{(\varphi,\lambda)}}{\gamma(0,\varphi)} * \frac{\partial T^c}{\partial r}|r = r_e \right. \quad (5)$$

R reference radius, GM-product of gravitational constant and mass of the earth. L, m degree, order of spherical harmonics, P_{lm}-fully normalized Legendre function C_{lm}^{W}, S_{lm}^{W} Stokes coefficient (fully normalized)(Barthelmes, 2013)

2.5.2 The Gravity Disturbance

The gradient of the disturbing potential is called the gravity disturbance vector. The gravity disturbance δ_g is not the magnitude of the gravity disturbance vector (as one could guess) but defined as the difference of the magnitude (Hofmann-Wellenhof & Moritz, 2005)

The reason for this definition is the practical measurement process, where the gravimeter measures only |∇W|, the magnitude of the gravity, and not the direction of the plumb line.(Toth & Torge, 2008)

In spherical harmonics, the gravity disturbance is defined as the magnitude of the gradient of the potential at a given point minus the magnitude of the gradient of the normal potential at the same point.

$$\delta_g(h,\lambda,\phi) = \sqrt{([W_u(h,\lambda,\phi)]^2 + [W_v(h,\lambda,\phi)]^2 + [W_w(h,\lambda,\phi)]^2)} - \sqrt{([U_u(h,\lambda,\phi)]^2 + [U_v(h,\lambda,\phi)]^2 + [U_w(h,\lambda,\phi)]^2)} \quad (6)$$

To calculate the gravity disturbance from eq. (6) the gradients ∇W and ∇U in A have to be calculated from spherical harmonics. The gradient ∇W in spherical coordinates is (e.g., Bronshtein et al., 2004): The spherical approximation δ_{gsa} of the gravity disturbance (eq. 6), i.e., the (negative) radial derivative of the disturbing potential T, calculated from a spherical harmonic expansion of T is:

$$\Delta g_{sa}(r,\lambda,\varphi) = \frac{GM}{r^2}\sum_{l=0}^{lmax}(\frac{R}{r})\text{^}l\ (l-1)\sum_{m=0}^{l} p_{lm}(sin\varphi)(C_{lm}^{W}\cos m\lambda + S_{lm}^{W} sinm\lambda) \quad (7)$$

R reference radius, GM-product of gravitational constant and mass of the earth. L, m degree, order of spherical harmonics, P_{lm}-fully normalized Legendre function C_{lm}^{W}, S_{lm}^{W} Stokes coefficient (fully normalized)(Eshagh, 2017)

Gravity anomaly

The gravity anomaly (according to Molodensky's theory) is defined as the magnitude of the gradient of the potential on the Earth's surface minus the magnitude of the gradient of the normal potential on the telluroid (Earth's surface minus height anomaly).

$$\Delta g(h,\lambda,\phi) = \sqrt{[W_u(h,\lambda,\phi)]\text{^}2 + [W_v(h,\lambda,\phi)]^2 + [W_w(h,\lambda,\phi)]^2} - \sqrt{\sqrt{[U_u(h,\lambda,\phi)]\text{^}2 + [U_v(h,\lambda,\phi)]^2 + [U_w(h,\lambda,\phi)]^2} \quad (8)}$$

The calculation of Δg at a given point (h, λ, φ) is possible if the height anomaly ζ has been calculated beforehand.(Ah & Akhter, 2009)

2.6 The determination of the geoid

The determination of the geoid is a purely physical problem. If we knew the mass density distribution within the Earth, we could compute the gravity field, including the gravity potential and thus the geoid, to any accuracy anywhere by using Newton's integration. We would then get the geoid by simply connecting the points of the same required value W_0 of potential. Unfortunately, we do not know the density distribution within the Earth with sufficient accuracy to do this, so this approach cannot be used in practice. The only viable alternative is to use gravity values, which are cheap, plentiful, and sufficiently accurate. If we have these, we can take advantage of the relationship between gravity and gravity potential (Kingdon et al., 2012)as shown in Fig. 5.

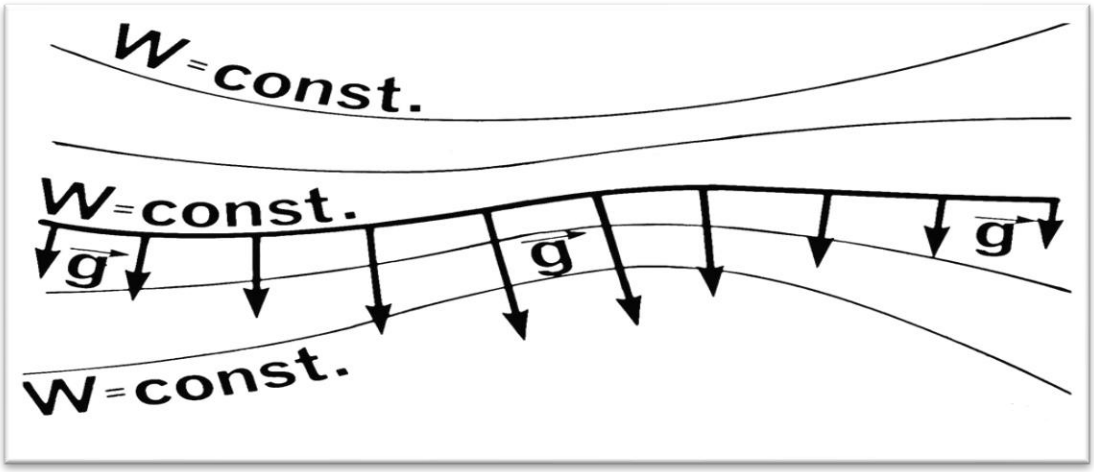

Figure 2.5 The relation between gravity and its potential

2.7 Methods of gravity reduction

2.7.1 Free-air reduction

The simplest assumption for gravity reduction is to neglect all topographic masses between the surface point P_S and its footprint on the geoid P. Gravity has to be downward continued along the plumb line between P_S and P over a distance H, the orthometric height of p_s. These types of reduction are known as free-air reduction. In linear approximation,

$$g_p^{FA} = g_{P_s} - \frac{\partial g}{\partial h}|p^{H_P} \qquad (9)$$

F_A stands for the free-air gradient. The gravity gradient depends on the location and the actual gravity field. To have a uniform definition of free-air gravity, a fixed value is taken. In this case, F_A comes from the simplification:-

$$g \approx \frac{GM}{r^2}\frac{\partial g}{\partial r} = -2\frac{G\,M}{r^3} = -2\frac{g}{r} \quad (10)$$

Inserting the numbers, we get:

$$g_p^{FA} = g_{P_s+} FA.H_p \quad (11)$$

With $FA = 0.30386\,{}^{mGal}/_{m}$ H (12)

The gradient is expressed in *gal/m*. Thus, the heights are expressed in meters and gravity values in gal. Note that F_A is positive. Gravity increases towards the center of the Earth. In Calculating the free-air gravity field, the topography is neglected, particularly its gravitational attraction. This shows up in the reduced gravity field *g* correlation with the original topography. This is unwanted for geoid computations. The topography must be considered differently.(Poutanen, 2020)

2.7.2 Bouguer reduction

During the famous French arc measurement expedition to Peru, Bouguer noticed the correlation between gravity and the topography of the Andes. The reduction of gravity by topography is named after him: *Bouguer reduction*.

Bouguer Plate is the simplest form to approximate the topography surrounding point P_S *by* an infinite plate of thickness *H,* a Bouguer plate. This does not imply the model of the whole region by such a plate. On the contrary, at each terrain point, a new plate is considered. The Bouguer plate can be considered a cylinder of height *H* and infinite radius.

g (Bouguer plate) = $2pGrH_P$

$$BO = \frac{\partial g}{\partial h}(B * p) = -2pGr = -0.1119mG * H \quad (13)$$

The latter quantity was derived from the conventional crustal density $r = 2670kg/m^3$. The Bouguer gradient BO, which is also expressed in *mgal*, *m*, is negative because gravity becomes less if the plate is removed.(Hofmann-Wellenhof & Moritz, 2005)

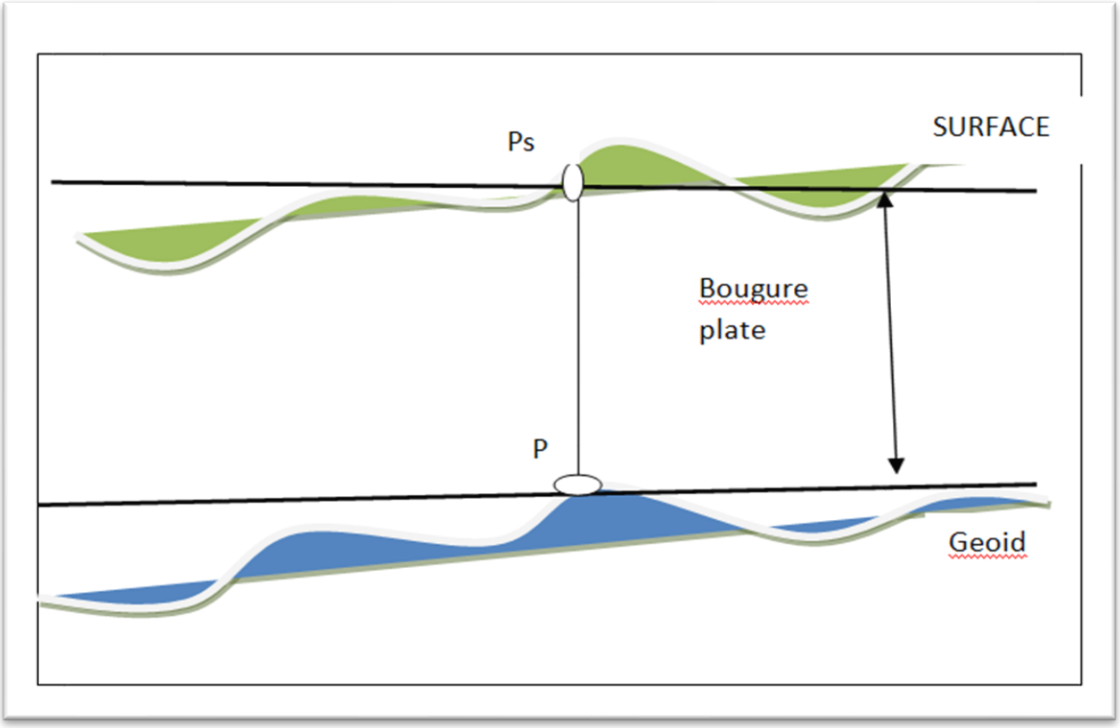

Figure 2.6 Bouguer plate: modeling the topography pointwise of an infinite slab of thickness H

2.8 Gravity mission satellite data

2.8.1 GOCE satellite data

The Gravity Field and Stable State Ocean Circulation Explorer mission is considered complementary to the CHAMP (launch July 15, 2000) and GRACE (launch March 17, 2002) missions. The precise orbit of a satellite with respect to a particular reference plane, the geoid, can be calculated using knowledge of the Earth's gravitational field. The mapping of ocean and land surfaces and high-accurate point locations utilizing satellite techniques are thus strongly coupled. To better comprehend the processes taking place within the Earth's interior as well as on and above its surface, Earth sciences provide a second justification for figuring out the Earth's gravity field. With a spatial resolution of at least 100 km, the Gravity Field and Stable State Ocean Circulation Explorer gravity gradiometer can measure the gravity field; however, at longer wavelengths (over 700–1000 km), it is not very accurate. ((Bagherbandi & Tenzer, 2013)

2.8.2 GRACE Satellite Data

The processing of the Gravity Recovery and Climate Experiment data and the creation of Level-1 and Level-2 products is handled by four processing facilities, including the CNES5, Center for Space Research (CSR), Austin, TX, USA, GeoForschungs Zentrum (GFZ),

Potsdam, Germany, the Jet Propulsion Laboratory (JPL), Pasadena, CA, USA, and the Science Data Center (SDC). The Physical Oceanography Distributive Active Data Center (PODAAC) at JPL and the GFZ's Integrated System Data Center (ISDC) both provide these goods. The SDC regularly pre-processes Level 1 Gravity Recovery and Climate Experiment data, which consists of location and velocity measurements made using GPS accelerometer data and KBR inter-satellite measurements, as well as monthly global GRACE gravity solutions (Level 2). These latter solutions are based on Stokes coefficients, which are dimensionless spherical harmonics or coefficients of the geopotential, produced up to a degree between 50 and 120 and corrected using along-track Gravity Recovery and Climate Experiment measurements. The monthly Gravity Recovery and Climate Experiment solutions are calculated using a dynamical method based on the Newtonian formulation of the satellite's equation of motion in an inertial reference frame centered on the Earth, in conjunction with specialized modeling of the gravitational and non-conservative forces acting on the spacecraft. (Journal, 2008)

The Gravity Recovery and Climate Experiment coefficients are calculated to remove the barometric redistribution of mass variations in both the atmosphere and the ocean, using data from the European Center for Medium-Range Weather Forecasts (ECMWF) and National Centers for Environmental Prediction (NCEP) reanalysis for atmospheric mass variations and ocean tides, as well as global ocean circulation models. As a result, there are the Gravity Recovery and Climate Experiment Coefficient Reversals, which are supposed to represent errors in the correction of the models and noises while also primarily storing continental water. Additionally, because to variations in the way data is processed, the correction models picked, and the data chosen to calculate the monthly average, monthly Gravity Recovery and Climate Experiment solutions vary from one official supplier to the next. (Chanard et al., 2014)

The Gravity Recovery and Climate Experiment K-band ranging inter-satellite observations provide precise information on a low-frequency gravity spectrum. (B a g h e r b a n d i & T e n z e r , 2 0 1 3)

2.9 Estimation of geoid to quasi-geoid separation

A spectral representation of the gravity field using spherical harmonics is used in the derivation of gravity field quantities from the GGM coefficients. The following expression is used to calculate the disturbing potential T, which is the difference between the Earth's gravity potential (W) and the normal gravity potential (U) at any point (r, Ω). (Hofmann-Wellenhof & Moritz, 2005)

$$T(r,\Omega) = \sum_{n=2}^{\bar{n}\,max}(\frac{R}{r})\text{^}n + 1 \sum_{m=-n}^{n} T_{n\,m}\, Y_{nm}(\Omega) \qquad (14)$$

where R = 6371 × 10^3 m is the Earth's mean radius (which approximates the geocentric radius of the geoid surface), $Y_{n,m}$ is the (fully normalized) spherical harmonic functions of degree n and order m, T_{nm} is the (fully normalized) coefficients of the disturbing potential, and n_{max} is the upper summation index of spherical harmonics. The 3-D position is defined in the system of spherical coordinates (r, Ω), where r is the spherical radius and Ω = (φ, λ) denotes the spherical direction with the spherical latitude φ and longitude λ. The geoid height N is defined by the well-known Bruns' (1878) formula in the following form

$$N(r,\Omega) = \frac{T(r_g,\Omega)}{\gamma_o\,(\phi)} \tag{15}$$

where γ_o is the normal gravity calculated at the reference ellipsoid using, for instance, Somigliana's (1929) formula. The disturbing potential T in Eq. (7) is computed at the geoid surface. The geocentric radius of the geoid surface is denoted as r_g.

By analogy with Eq. (7), the quasi-geoid height ζ (i.e., the height anomaly) is defined as (Molodensky et al., 1960

$$\zeta(r,\Omega) = \frac{T(r_p,\Omega)}{\gamma_o\,(\phi)} \tag{16}$$

Where γ_o is the normal gravity of the telluroid. The computation of the normal gravity value γ_o can be done according to the expression given in Heiskanen and Moritz [1967]. The disturbing potential T is in this case calculated at the surface point. The geocentric radius of the surface point is denoted as R_P.

The geoid-to-quasi-geoid correction is defined approximately as a function of the simple planar Bouguer gravity anomaly Δg^{SB} and the topographic height H of the computation point. With reference to Heiskanen and Moritz (1967), we write

$$\zeta(\Omega)\text{-}N(\Omega)\cong\text{-}\Delta g^{SB}(r,\Omega)/\gamma(\Omega)\ ^*H(\Omega) \tag{18}$$

Where γ is the integral mean of the normal gravity along the normal between the reference ellipsoid and the telluroid.The simple planar Bouguer gravity anomaly Δg^{SB} in Eq. (5)

$$\Delta g^{SB}\left(r_{p,}\Omega\right) = \Delta g(\left(r_{p,}\Omega\right) - 2\pi G\rho_0^t\,H(\Omega) \tag{19}$$

Where G = 6.674 × 10^{-11} m^3 kg^{-1} s^{-2} is Newton's gravitational constant, $\rho_0{}^t$ is the mean topographic mass density, and Δg is the (free-air) gravity anomaly. We note that either the normal or orthometric heights can be used to compute both the geoid-to-quasi-geoid correction in Eq. (18). and the Bouguer gravity anomaly [in Eq. (13)] A more accurate expression for computing the geoid-to-quasi-geoid correction in the spectral domain was given by(Tenzer, Novák, et al., 2006); see also(Bagherbandi & Tenzer, 2013). It reads.

$$\zeta(\Omega) - N(\Omega) \cong \frac{T(r_p,\Omega)}{\gamma_Q(\phi)} - \frac{T(r_g,\Omega)}{\gamma_o(\phi)} - \frac{V^1_{bias}(r_p,\Omega)}{\gamma_Q(\phi)} \quad (20)$$

The last constituent on the right-hand side of Eq. (20), i.e., (V^t_{bias}/γ), defines the topographic bias. This bias represents the error in the analytical downward continuation of the external gravitational potential inside the topographic masses. For the adopted constant topographic mass density distribution, the term V^t_{bias} is computed according to the following spectral expression (Sjöberg, 2008)

$$V^1_{bias}(r_p,\Omega) = 2\pi G\rho^t_0 \sum_{n=0}^{\bar{n}\,max}\sum_{m=-n}^{n}(H^{(2)}_{n,m} + \frac{2}{3R}H^{(3)}_{n,m})Y_{n,m}(\Omega) \quad (21)$$

The computation of the topographic bias in the spectral domain is numerically stable when using a low-degree series as cited by Ågren (2004) and Sjoberg (2007), however, demonstrated that the computation became unstable at a very high degree spherical harmonic term of a power series of topographic the terms:$\left\{\sum_{n=m}^{n} H^{i}_{n\,m} Y_{n\,m}(\Omega): i = 1,2,3\right\}$ in equation define the spherical height function

$$\{H^i_n : i = 1,2,3\} \text{ i.e } (H^{(i)}_n(\Omega) = \frac{2n+1}{4\pi}\iint_{\Phi} H^t(\grave{\Omega})P_n(t)d\grave{\Omega} = \sum_{m=-n}^{n}(H^{(i)}_{n,m}Y_{n,m}(\Omega) \quad (22)$$

Where P_n is the Legendre polynomial of degree n with the argument t equal to the cosine of the spherical distance ψ between the spherical directions(Ω) and Ω;i.e, t:t=cosψ (Bagherbandi & Tenzer, 2013).

2.9.1 Determination of N- ζ using Sjöberg's equation

The second method to calculate N- ζ is the accurate equation of (Sjöberg, 2010)as follows, which consists of three parts:

$$\zeta(\Omega) - N(\Omega) \approx \frac{\Delta g_p^{Bo}}{\gamma} * H^O + \frac{vg^t - vp^{pt}}{\gamma} + \frac{\delta g^{BO-} - \delta g_p^{BO-}}{\gamma} \quad (23)$$

The right-hand side of Eq. (23), i.e., (V^t_{bias}/γ), defines the topographic bias .The first part $\frac{\Delta g_p^{SB}}{\gamma} * H^O$ is known as the approximate equation of Featherstone and Kirby (1998) in which vg^T the topographic potential around the point is located on the geoid and vp^T is the computed topographic potential around P on the earth's surface the third part,$\frac{\delta_g^{-BO} - \delta_{gp}^{BO}}{\gamma}$, in which is the difference between the average of gravity distribution between the earth surface and the geoid, $\frac{\Delta g_p^{Bo}}{\gamma}$ denotes (simple) Bouguer gravity anomaly at the computation point P on the earth surface obtained from the following equation (Hofmann-Wellenhof & Moritz, 2005).

$$\frac{\Delta g_p^{Bo}}{\gamma} = g\ + 0.3086H - 0.1119H - \gamma \quad (24)$$

Here, H is the orthometric height, g is the observed gravity on the earth's surface, and γ refers to the ellipsoidal normal gravity. It is worth mentioning equation (24) was proposed by Flury and Rommel (2009), but the last term of equation (24) was not contained in their final formulation. To compute Bouguer gravity anomaly, the values of the above-mentioned variables, i.e., g, H, and γ, have been gained from the ICGEM website, which is estimated based on a combination of satellite and land data. Furthermore, the Bouguer gravity anomaly at point P on the earth is accessible on the ICGEM website directly; γ is the average of normal gravity from the geoid to the reference ellipsoid or from the earth's surface to quasi-geoid which can be computed by the following equation (Heiskanen and Moritz, 1967).

$$\gamma = \gamma_{po}\left[1 - (1 + f + m + 2f + \sin^2\varphi) * \frac{H}{a} + \frac{H^2}{a^2}\right] \quad (25)$$

Where f = 0.00335281068118 is the geometrical flattening, m = 0.00344978600308 is Kloro constant, a = 6356752.3141m is the ellipsoid semiaxis, φ is the latitude of P and γ_{po} normal gravity of ellipsoid and is determined using Pizzertti (1894) formula

$$\lambda_e = \left(1 + \beta_1 \sin^2\ \varphi\ + \beta_{1\sin^2 2\varphi}\right) \quad (26)$$

Where $\lambda_e$refers to normal gravity at the equator and β $_1$ 0.0053024 and a_β_2=0.0000059

The second part is $\frac{vg^T - vp^T}{\gamma}$ (Hofmann, Moritz ,et al., 2017) where vg^T the topographic potential around the point is located on the geoid and vp^T is the computed topographic potential around P on the earth's surface which has been calculated using the prism formula proposed by Nagy et al. (2000)

Finally, the third part,$\frac{\delta_g^{-BO} - \delta_{gp}^{BO}}{\gamma}$, in which is the difference between the average of gravity distribution between the earth surface and the geoid, and the gravity distribution at measuring point P as normalized by the γ Bouguer distribution on the earth surface is estimated as follows

$$\delta_{gp}^{BO} = g_p - \gamma_p \quad (27)$$

Here, g_p is the calculated gravity at P point on the earth and $\gamma_p$is the measured normal gravity at P on the earth's surface. In measure, γ_p can be written in the following form (Moritz, 1992).

$$\gamma_p = \gamma_{po}[1 - 2(1 + f + m - f sin^2\varphi)\frac{h}{a} + 3\left(\frac{h}{a}\right)^2] \quad (28)$$

Here, h is the ellipsoidal height of the point. The value variables in the recent formulas have been gained from the ICGEM website. It is worth mentioning that the WGS84 reference ellipsoid has been employed in all calculations. And,

$$\gamma_g^{-BO} = \frac{\delta g_P^{BO} + \delta g_{po}^{BO}}{2} \quad (29)$$

$$\delta g_P^{BO} = g_p + 0.3086h - 0.1119h - \gamma_{p0} \quad (30)$$

Where h is the ellipsoidal height (gained from the mentioned site) and γ_{p0} has already been calculated (Pellinen, 1972).

CHAPTER THREE

3. Methodology and Materials

3.1 Study area

On the African continent, Ethiopia is home to some of the most distinctive sites. In comparison to other African nations, Ethiopia currently has the most UNESCO World Heritage sites. Ethiopia preserves the past by preserving unusual and stunning ruins that date back hundreds of years. The stunning landscape of Ethiopia varies from the Danakil depression, one of the hottest places on earth, which is 117 meters below sea level, to the forested highlands of Siemen Mountain National Park, which reach an elevation of 4,620 meters above sea level at the famous mountain summit known as Ras Dashan (Dejen). The highest mountain peak in Africa and fourth in Ethiopia is Mount Ras Dashen (Dejen). Due to its abundance of mountains that rise more than 4,000 meters above sea level, Ethiopia is commonly referred to as "The Roof of Africa." Ethiopia is often referred to as the "water tower of East African countries" due to the fact that the majority of its rivers flow down to other African nations. The massive Blue Nile, Tekez e, and Wabe Shebele Rivers are only a few of the rivers that leave Ethiopia's borders.(Austin, 2016)

Ethiopia has several national parks, one of which is the Simien Mountains National Park. Its area spans the Semin Mountains and includes Ras Dashan (Dejen), Ethiopia's highest point, and is situated in the Siemen (North) Gondar Zone of the Amara Region. Several threatened species call it home, including the Ethiopian wolf and the wail ibex, a wild goat that is unique to this region only. The Gelada baboon and the caracal, a cat, are both found in the Simien Mountains. The park is home to more than 50 different bird species, including the spectacular lammergeyer, or bearded vulture, with its 3 m (10 ft) wingspan. (Plan, 2015)

An unpaved road crosses the park from Debarq, where the administrative center of the park is located, east through a number of settlements to the Buahit Pass (4,430 m), where the road swings south to and at Mekane Berhan, 10 kilometers beyond the park boundaries. (Gile et al., 2018)

3.1.1 Location

Simien Mountains National Park (SMNP) is located boundaries of 13^{0}06' 44.09" N to 13^{0}23' 07.85" N latitude and 37^{0}51'26.36" E to 38^{0}29' 27.59" E longitude. 2015's African Wildlife

Foundation It is a part of the Amara Regional State's North Gonder Zonal Administration. The national park is bordered by about four KAs from AdiArkay woreda in the north, seven KAs from Debarq woreda in the west, fifteen KAs from Beyeda woreda in the northeast and east, nine KAs from Jan Amora woreda in the south, and three KAs from Tselemt woreda in the north-east.(Chernet, 2015).

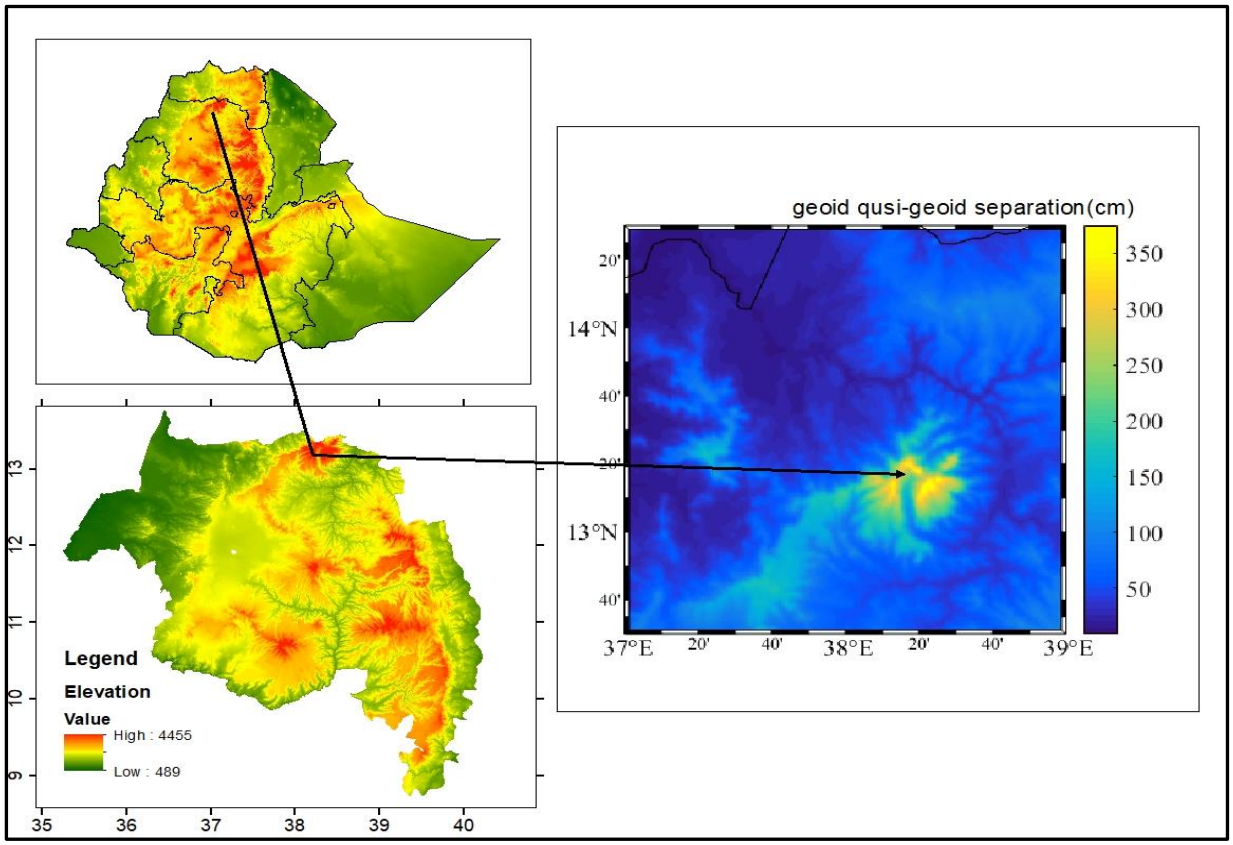

Figure 3.1 Location of Semien plateau

3.1.2 Topography

According to Figure 2, the elevation of SMNP varies from 1900 meters in the northwestern region to 4533 meters in the far southwest. The majority of these regions' northern sides are occasionally extremely steep. The highest and mean slope classifications in the Simien Mountains national park were 76.83 and 25.31 degrees, respectively, with a standard deviation of 13.97.(Chernet, 2015)

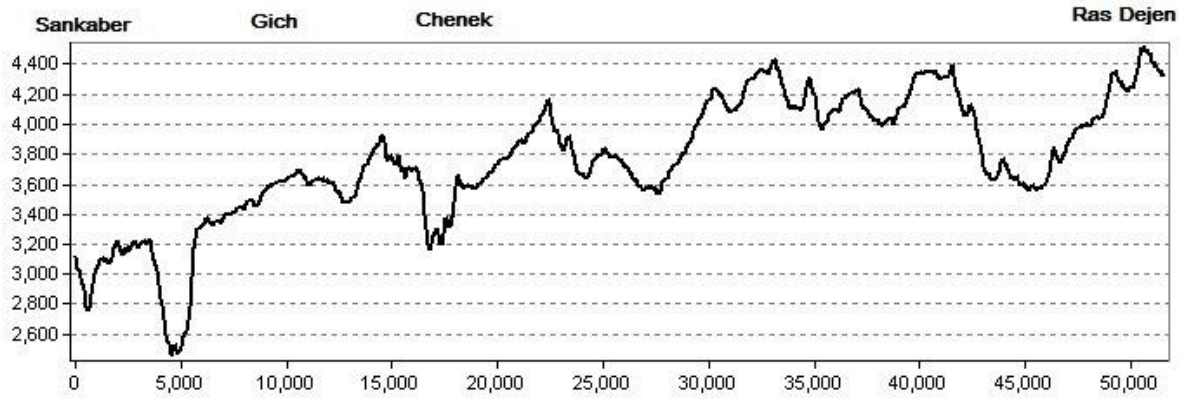

Figure 3.2 Profile graph: Sankaber-Gich-Chenek-Ras Dejen at SMNP

3.1.3 Climate

There is a rainy and dry season in the Simien Mountains, with around 75% of the yearly rainfall occurring between June and September. The SMNP is located in an isohyet with an average annual rainfall of 1,500 mm at 3,600 mean sea level, or between 1,350 and 1,600 millimeters. Although there is a significant diurnal difference, with minimums of -2°C to -4°C at night and maximums of 11°C to 18°C during the day, temperatures are generally consistent throughout the year. The Simien Mountains' climate can generally be divided into four altitude-based climate zones: the Wurch zone, with an alpine climate above 3,700 meters above sea level; the High Dega zone, with a cool climate between 3,400 and 3,700 meters above sea level; the Dega zone, with a temperate climate between 2,400 and 2,400 meters above sea level; and the Woina Dega zone, with a subtropical climate between 1,500 and 2,400 meters above sea level. (Plan, 2015)

3.2 Data source

The Gravity Recovery and Climate Experiment and GOCE satellite data models that we chose from the models offered by CNES to utilize in this study are the data that we used. The degree, the kind of satellite data used, and the time they were created are used as identification criteria for the data. As shown in the table 3.1 below, the models employed in this investigation are as follows.

3.2.1 GRACE data

The Graz University of Technology's most recent Gravity Recovery and Climate Experiment - only gravity field model, ITSG-Grace2018, provides unconstrained monthly and regularized daily solutions in addition to a long-term static field. Sets of spherical harmonic coefficients

for various maximum degrees (60, 96, and 120) were calculated in each month of the observation period without using any regularization. A set of spherical harmonic coefficients up to degree and order 40 was co-estimated in order to accurately resolve high-frequency gravity field changes. As observations, K-band range rates with a sampling of 5 seconds and kinematic orbits with a sampling of 5 minutes were used. The kinematic orbits of the Gravity Recovery and Climate Experiment satellites(Klinger & Mayer-gürr, n.d.) Using the GPS orbit and clock solutions supplied by CODE, the processing was completed. Moreover, a complete accelerometer scale factor matrix was computed daily (Klinger and Mayer-Gürr, 2016). With a six-hour node interval and predicted for each axis and day, the accelerometer bias was modeled using cubic splines. On http://ifg.tugraz.at/ITSG-Grace2018, you can find information on ITSG-Grace2018. The statistics range from April 2002 to August 2016 and are available on a monthly and daily basis.(Mayer-Gürr et al., 2018)

3.2.2 Data from the GOCE satellite

It assemble the Gravity Field and Stable State Ocean Circulation Explorer only satellite model, GO_CONS_GCF_2_TIM_R6, to a spherical harmonic degree of 300 using Satellite Gravity Gradiometry (SGG) data and Satellite-to-Satellite Tracking (SST) observations along the Gravity Field and Stable State Ocean Circulation Explorer orbit.

Four data models made available by CNES were employed in this study to make side-by-side comparisons. To evaluate the anticipated improvement of the gravity field at medium wavelengths, the GO_CONS_GCF_2_TIM_R6 gravity field quantities are calculated. (Kvas et al., 2021)

3.2.3 Data from the GOCE and GRACE satellite

1. The SGG-UGM-2 model

Compared to other model in the frequency and spatial domains, the SGG-UGM-2 model shows a promising performance in the GPS/leveling validation and error analysis. Along with the models SGG-UGM-1, SGG-UGM-2, EIGEN-6C4, and GECO the GPS/leveling data from China and the United States are utilized to validate these models. The statistics of the discrepancies between model-derived quasi-geoidal/geoidal heights and GPS/leveling data, along with their histograms and empirical variograms, show that SGG-UGM-2 performs the best in the United States. SGG-UGM-2 has a somewhat superior performance than its

predecessor SGG-UGM-1 in the Chinese mainland, the United States, and the Chinese coastal city of Qingdao thanks to the contribution of the new GRACE NEQ and the new marine gravity anomalies. As a result, it can be concluded that the techniques employed to create SGG-UGM-2 are sound and can be applied to the creation of upcoming SGG-UGM series using independent terrestrial gravity datasets that are now available (for example, the Chinese mainland). Furthermore, the new model SGG-UGM-2's accuracy suggests that this model will give users a different option.(Liang et al., 2020)

2. The gravity field model IGGT_R1

The GOCE, IGGT by least squares approach was used to create the gravity field model IGGT_R1. This model avoids mistakes brought about by faulty measurements of the satellite's attitude during the conventional coordinate transformations because of the unique properties of IGGT. The geostrophic velocity speeds in the Agulhas current area suggest that IGGT_R1, which provides more information about the Gravity Field and Stable State Ocean Circulation Explorer, GGs, is a better option than EIGEN-5C. The earliest gravity field models from ESA, IGGT_R1, contain the same Gravity Field and Stable State Ocean Circulation Explorer GGs after laborious calculations using the least squares method.(Lu et al., 2018).

Table 3.1 Data from the Global Gravity Field Model

no	Model Name	Year	Degree	Model	Reference
1	SGG-UGM-2	2020	2190	A, EGM2008, Grace), S (Goce)	Liang, W. et al. 2020
2	IGGT_R1C	2018	240	G, S(Goce), S(Grace)	Lu, B. et al., 2018
3	GO_CONS_GCF_2_TIM_R6	2019	300	S(Goce)	Brockmann, J. M. et al, 2021
4	ITSG-Grace2018s	2019	200	S(Grace)	Mayer-Gürr, T. et al, 2018

3.2.3 Topography data

ETOPO1 is a 1 arc-minute global relief model of Earth's surface that integrates land topography and ocean bathymetry. Built from global and regional data sets, it is available in "Ice Surface" (top of Antarctic and Greenland ice sheets) and "Bedrock" (base of the ice sheets). (https://doi.org/10.25921/fd45-gt74.)

3.3 Research plan

To accomplish the necessary goals in this study, qualitative data sets gathered from secondary data sources were utilized. Space-borne data from various satellite missions (EGM 08, Gravity Field and Stable State Ocean Circulation Explorer, and Gravity Recovery and Climate Experiment satellite data) is one of these data sources. For the data analysis, a variety of tools and software programs have been employed. After the data set was analyzed using the aforementioned analysis tools, the results were presented in the form of tables, figures, and text. Some of the software is GIS, MATLAB, Graf Lab, Graph soft, etc.

3.4 Methods of Data Analysis

3.4.1 Determination of computation Area grids by using MATLAB and GIS

The location of the geoid to quasigeoid separation computation cover from 37^0E to 39^0E longitude and from 12.5^0 N to 14.5^0 N latitude.

The Global Gravitational Models play an important role in determining geoid and quasi-geoid heights. They are responsible for the long wavelength and short wavelength information of the gravity field. In this paper, they used the Gravity Field and Stable State Ocean Circulation Explorer based model and the Gravity Recovery and Climate Experiment based model. Details about the International Center for Global Earth Models data center (IGGT_R1C, SGG-UGM-2, GO_CONS_GCF_2_TIM_R6, ITSG-Grace2018s GRACE ,and Gravity Field and Stable State Ocean Circulation Explorer models) used to compute gravity field data for the Semien plateau,(Rase Dejen) study area (Ince et al., 2019) (https://www.icgem.gfz-potsdam.de/).

The GGMs were downloaded from the International Center for Global Earth Models (Ince et al., 2019) (https://www.icgem.gfz-potsdam.de/) data center (IGGT_R1C, SGG-UGM-2, GO_CONS_GCF_2_TIM_R6, ITSG-Grace2018s GRACE ,and GOCE model) to compute gravity field data for the study area.

Gravity field computation using GGM models' spherical harmonics (IGGT_R1C, SGG-UGM-2, GO_CONS_GCF_2_TIM_R6, and GRACE and Gravity Field and Stable State Ocean Circulation Explorer models from ITSG-Grace2018).The gravity field models IGGT_R1C, SGG-UGM-2, GO_CONS_GCF_2_TIM_R6, ITSG-Grace2018s GRACE ,and Gravity Field and Stable State Ocean Circulation Explorer mode), and the topography model ETOPO1 (Ice Surface) (Amante & Eakins, 2009), have been used to calculate the described functional and their approximations on global grids. The resolution of the grids is 0.01 ◦×0.01 ◦ and the models IGGT_R1C2, GO_CONS_GCF_2_TIM_R6, ITSG-Grace2018s GRACE and Gravity Field and Stable State Ocean Circulation Explorer models have been evaluated up to their maximum degree of l_{max} = 200, and, SGG-UGM model has been evaluated up to its maximum degree of l_{max} = 2190. All calculations are carried out concerning the reference system WGS84. The differences between the models of the same function are presented.

The computation of the gravity field uses the reference system of WGS 84. The constant parameter GM, reference point 3.98600441800x1014m3/s2, the radius of reference point 6378137.00m, flatting of the reference point 3.35281066474748x10-3 (1/98.25722356300), omega reference 7.29211500000E-05 1/s, normal potential 6.263685171456948E+07 m2/s2. The computation area extends from 14.5 degrees north to 12.5 degrees south, and from 37 degrees west to 39 degrees east, with 0.01-degree steps. The maximum grid to compute gravity fields is 40401 grids on Semien plateau. The maximum degree used to compute the gravity field of Semien plateau,(Ras Dejen)is 200 and, as a comparison, used 2190 for one GGM model. The computation of gravity field data used the GGM model from the ICGEM.(Moritz, 1992)

3.4.1 Computation of gravitational function using a gravity earth model

Equations (2) and (3) outline how to determine the gravity potential using the earth's geopotential gravity model based on the mountain's stock coefficient. In real-world situations, this can be helpful. The notations are the computation point's spherical geocentric coordinates (radius, longitude, and latitude), with R standing for the reference radius, GM for the product of the earth's mass and gravitational constant, L,m for degrees and order, and p_{lm} for the order of spherical harmonic The following equation describes how the geopotential's spectral and spatial domains are related:-

$$W_a(r,\lambda,\varphi) = \frac{GM}{r}\sum_{l=0}^{l_{max}}\sum_{m=0}^{l}\left(\frac{R}{r}\right)^{l} p_{lm}(sin\varphi)(C_{lm}^{W}cosm\lambda + S_{lm}^{W}sinm\lambda)$$

This shows the 1/r-behavior for r → ∞, written in the form

$W_a(r,\lambda,\varphi) = \frac{GM}{r}\sum_{l=0}^{l_{max}}\sum_{m=0}^{l}(\frac{R}{r})^{l+1}\, p_{lm}(sin\varphi)(C_{lm}^{W}cosm\lambda + S_{lm}^{W}sinm\lambda$

L, m degree, order of spherical harmonics, P_{lm}-fully normalized Legendre function C_{lm}^{W}, S_{lm}^{W} Stokes coefficient (fully normalized)

The transformation formulas between ellipsoidal (h,λ,φ) and spherical(r,λ,φ)) coordinates can be found, e.g., in A spherical harmonic approximation of the gravity field up to a maximum degree l_{max}(a so-called "gravity field model") consists of (l_{max} + 1+1) ^2 coefficients and 2 values of GM and R to which the coefficient functions.

Additionally, the topographical model can be converted into a surface spherical harmonics expansion and used with equations (14) and (15) to calculate the geoid height N, which is determined by the well-known Burns' (1878) definition.

$T(r,\Omega) = \sum_{n=2}^{\bar{n}\,max}(\frac{R}{r})\text{^}n + 1\sum_{m=-n}^{n} T_{n\,m}\, Y_{nm}(\Omega)$ and The geoid height N is defined by the well-known Bruns' (1878) formula in the following form

$N(r,\Omega) = \frac{T(r_g,\Omega)}{\gamma_o\,(\phi)}$

where γ_o is the normal gravity calculated at the reference ellipsoid using, for instance, Somigliana's (1929) formula.where R = 6371 × 10^3 m is the Earth's mean radius (which approximates the geocentric radius of the geoid surface), $Y_{n,\,m}$ is the (fully normalized) spherical harmonic functions of degree n and order m, T_{nm} is the (fully normalized) coefficients of the disturbing potential, and n_{max} is the upper summation index of spherical harmonics.By analogy with Eq. (7), $\zeta(r,\Omega) = \frac{T(r_p,\Omega)}{\gamma_o\,(\phi)}$ the quasi-geoid height ζ (i.e., the height anomaly) is defined as (Molodensky et al., 1960.

The spherical approximation δ_{gsa} of the gravity disturbance (eq. 6), $\delta_g(h,\lambda,\phi) = \sqrt{([W_u(h,\lambda,\phi)]^2 + [W_v(h,\lambda,\phi)]^2 + [W_w(h,\lambda,\phi)]^2)} - \sqrt{([U_u(h,\lambda,\phi)]^2 + [U_v(h,\lambda,\phi)]^2 + [U_w(h,\lambda,\phi)]^2)}$ i.e., the (negative) radial derivative of the disturbing potential T, calculated from a spherical harmonic expansion of T is in eqtion 7:-

$\Delta g_{sa}(r,\lambda,\varphi) = \frac{GM}{r^2}\sum_{l=0}^{lmax}(\frac{R}{r})\text{^}l\,(l-1)\sum_{m=0}^{l} p_{lm}(sin\varphi)(C_{lm}^{W}\cos m\lambda + S_{lm}^{W}sinm\lambda)$

R reference radius, GM-product of gravitational constant and mass of the earth. L, m degree, order of spherical harmonics, P_{lm}-fully normalized Legendre function C_{lm}^{W}, S_{lm}^{W} Stokes coefficient (fully normalized) .The so-called "height anomaly" approximates the geoid according to Molodensky's theory. It is equal to the geoid over the sea. Here it will be

calculated, as defined on the Earth's surface approximated by Burns' formula on the ellipsoid plus a first-order correction. The elevation information is automatically taken from the ETOPO1 topography model. The calculation of the height anomalies ζ (ϕ, λ) by using equation 15 $\zeta(\mathrm{r},\Omega) = \frac{\mathrm{T}(\mathrm{r_p},\Omega)}{\gamma_o\,(\phi)}$ from the spherical harmonic potential model according to the iteration (eq. 4) $\zeta 1(\lambda,\phi) \approx \zeta e1(\lambda,\phi) + (\frac{h_t}{\gamma_0} * \frac{\partial T^c}{\partial h}|h = 0)$ is possible using and equation (5) $\zeta_1 = (\zeta_{e1} + \frac{H_{(\varphi,\lambda)}+(N_{(\varphi,\lambda)}}{\gamma(0,\varphi)} * \frac{\partial T^c}{\partial r}|r = r_e$ and by analogy with Eq. (7), $\Delta g_{sa}(r,\lambda,\varphi) = \frac{GM}{r^2}\sum_{l=0}^{lmax}(\frac{R}{r})\text{^}l\ (l-1)\sum_{m=0}^{l} p_{lm}(sin\varphi)(C_{lm}^W \cos m\lambda + S_{lm}^W sinm\lambda)$ the quasi-geoid height ζ (i.e., the height anomaly) is defined as (Molodensky et al. 1960) eq.5. To find the gravity field function.

3.4.2 Computation of the geoid-quasi-geoid separation

The geoid-quasi-geoid separation approximation formula from Featherstone and Kirby (1998) is given in equation (Eq. 23) $\zeta(\Omega) - N(\Omega) \approx \frac{\Delta g_p^{Bo}}{\gamma} * H^O$. By considering the revised Bouguer gravity anomaly, the gravity disturbance, and topographic surface sites for a computation of the geoid-quasi-geoid separation, Flury and Rummel updated this approximation. As a result, Sjoberg's exact formula was used to calculate it in this study using the geoid-quasi-geoid separation model. Using the ETOPO 1 and TC programs from the GRAVSOFT package, the gravity anomaly in the case area was determined. The ETOPO 1 provided the height of the computation point. The 0.01-degree spherical distance from the computational point served as the integration domain's boundary.These computation were done by satellite data model from ICEGM and E-TOPO 1 following the necessary steps. They contrast and investigate how they relate to one another.

Flow chart of computation of geoid quasi-geoid separation

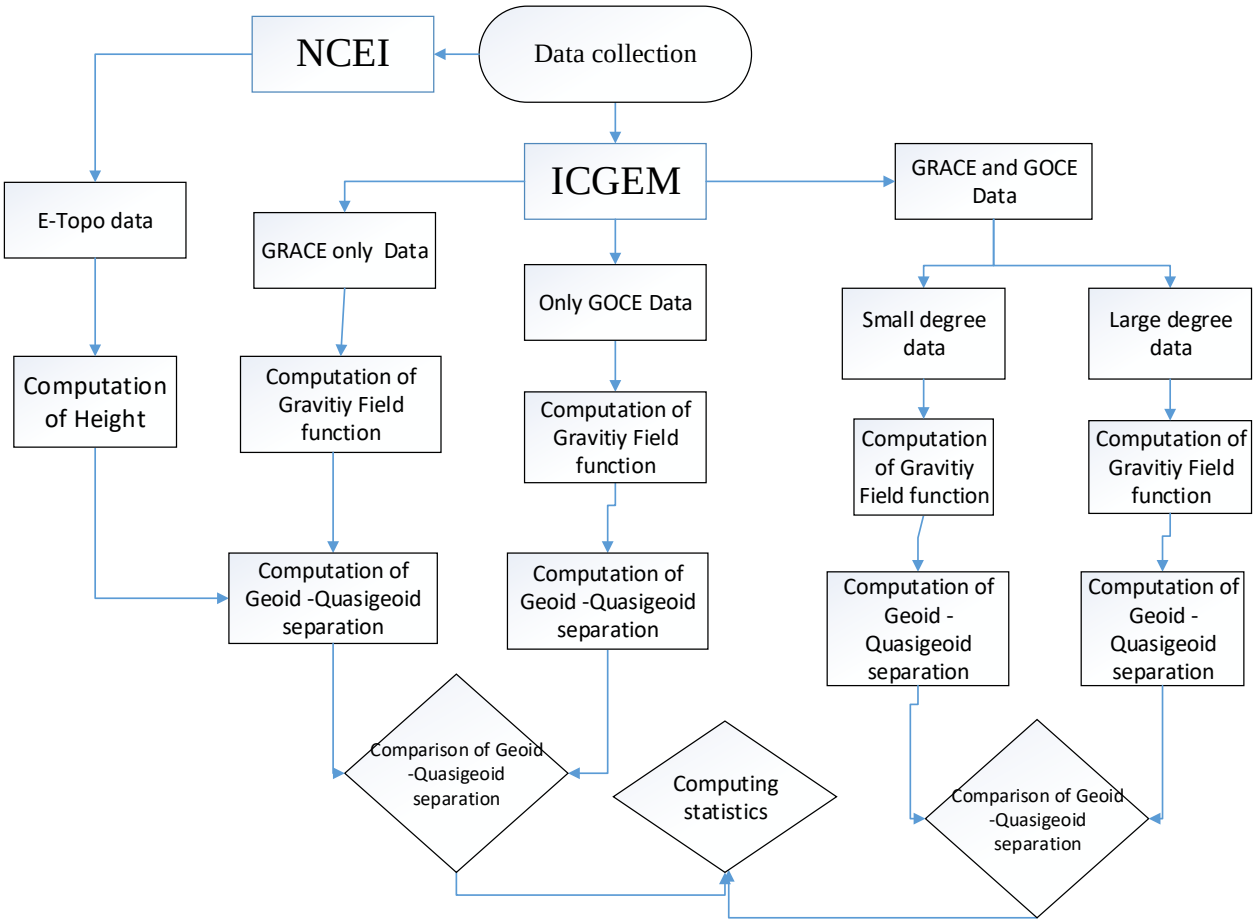

Figure 3.3 Procedure of geoid to quasi-geoid separation computation

CHAPTER FOUR

4. Result And Analysis

The results of handling and processing the data are shown in this section. The results were obtained using higher degrees of order model satellite data and a systematic process that relies on Gravity Recovery and Climate Experiment, Gravity Field and Stable State Ocean Circulation Explorer, and Gravity Recovery and Climate Experiment and Gravity Field and Stable State Ocean Circulation Explorer combined data to determine the geoid to quasi-geoid separation. the use of gravity-modeled data for the examination of geoid-quasi-geoid separation qualities in flat and hilly areas.

4.1 Gravity field computation from the gravity earth model

The WGS 84 reference system serves as the model's foundation. the constant parameter GM, the reference point's radius (6378137.00m), its flattening (3.35281066474748x10-3 (1/98.25722356300), its omega reference (7.29211500000E-05 1/s), and its normal potential (6.263685171456948E+07 m2/s2). With 0.01-degree steps, the computation region spans 14.5 degrees north to 12.5 degrees south and 37 degrees west to 39 degrees east. The calculation of the gravitational field is completed using 40401 as its total number grid. For comparing the Gravity Recovery and Climate Experiment and Gravity Field and Stable State Ocean Circulation Explorer gravity models, the geoid of Semien plateau (Ras Dejen) is calculated to a maximum degree of 200, and we additionally utilize 2190.The GGM model from the ICGEM was utilized to calculate gravity field data. The three models' gravity disturbances, which range from 0 to 36 mgal, are discovered in the same range as those reported in the four models with the identical formula. The ITSG-Grace2018s model, which is the only one produced by the Gravity Recovery and Climate Experiment satellite and is shown in Figure 4.1 (a), has a mean gravity disturbance of 7.123 mgal, a minimum gravity disturbance of 4.825 mgal, and a maximum gravity disturbance of 32.470 mgal. The model employed in Figure 4.1 (b) is called GO_CONS_GCF_2_TIM_R6 GOCE, and it exclusively makes use of the Gravity Field and Stable State Ocean Circulation Explorer satellite. Using the GO_CONS_GCF_2_TIM_R6 GOCE data model, the gravity disturbance has a mean of 7.129 mgal and minimum and maximum of 4.901 mgal.

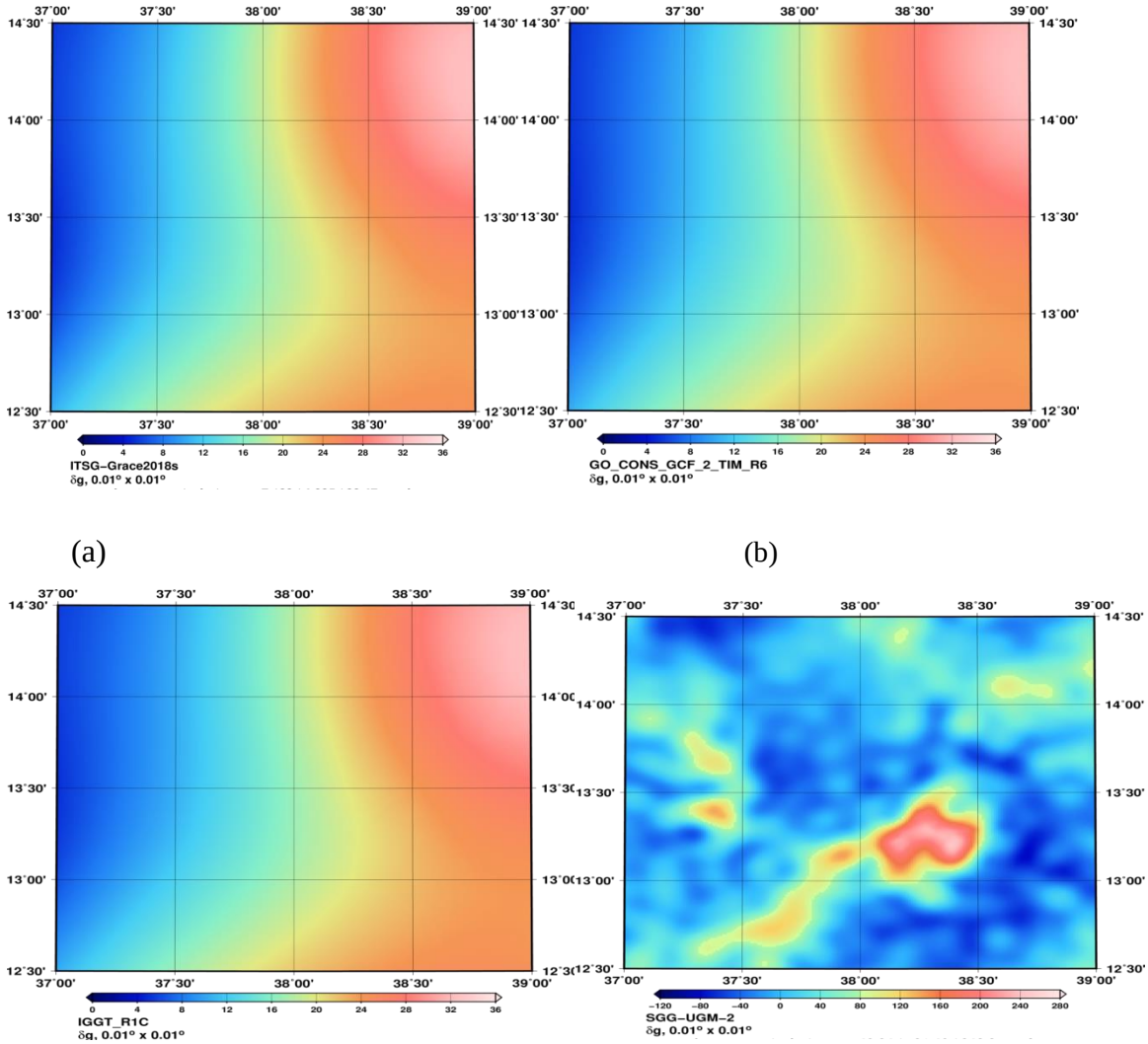

(a) (b)

(c) (d)

Figure 4.1.**(a) gravity disturbance in model ITSG-G, (b) gravity disturbance in model GO_CON, (c) gravity disturbance in model IGG_R1, (d) gravity disturbance in model SGG-U**

mgal and 32.32 mgal, respectively .The model IGGT_R1C shown in Figure 4.1 (c) is the result of the two satellite models, and in this model, the mean of the gravity disturbance is 7.160 mgal, and the minimum and maximum gravity disturbances are 5.130 mgal and 32.340 mgal respectively. When we look at the model SGG-UGM-2, as shown in Figure 4.1 (d), we see that the range level is different from others, ranging from -120 to 280 mgal. The model shown in Figure 4.1 (d), SGG-UGM-2, is the result of the two satellite models and is made to a high degree of the scale. In this model, the mean gravity disturbance is 49.840 mgal and the minimum and maximum gravity disturbances are -81.490 mgal and 243.200 mgal, respectively. A summary, the four model results are shown in Table 4.1 below.

Table 4.1. Summary of the gravity disturbance results of the four models

Gravity model	ITSG-Grace2018s model(mgal)	IGGT_R1C GRACE Model(mgal)	GO_CONS_GCF_2_TIM_R6 Model (mgal)	SGG-UGM-2 Model(mgal)
minimum	4.825	5.130	4.901	-81.486
maximum	32.470	32.340	32.320	243.159
mean	7.123	7.160	7.129	13.759

The gravity anomaly found in the four models with the same formula is found in the same range in the three models, which range from 0 to 36 mal. To compare the mean, minimum, and maximum, the ITSG-Grace2018s model shown in Figure 4.2 (a) is the only one made by the Gravity Recovery and Climate Experiment satellite, and in this model, the mean of the gravity anomaly is 7. 064mgal, with the minimum and maximum gravity anomaly being 5.441 mgal and 32.680 mgal, respectively. The model shown in Figure 4.2 (b) is GO_CONS_GCF_2_TIM_R6 GOCE, and only the Gravity Field and Stable State Ocean Circulation Explorer satellite is used. The mean of the gravity anomaly by using the GO_CONS_GCF_2_TIM_R6 GOCE data model is 7.129 mgal, and the minimum and maximum gravity anomaly s are 4.901 mgal and 32.320 mgal respectively.

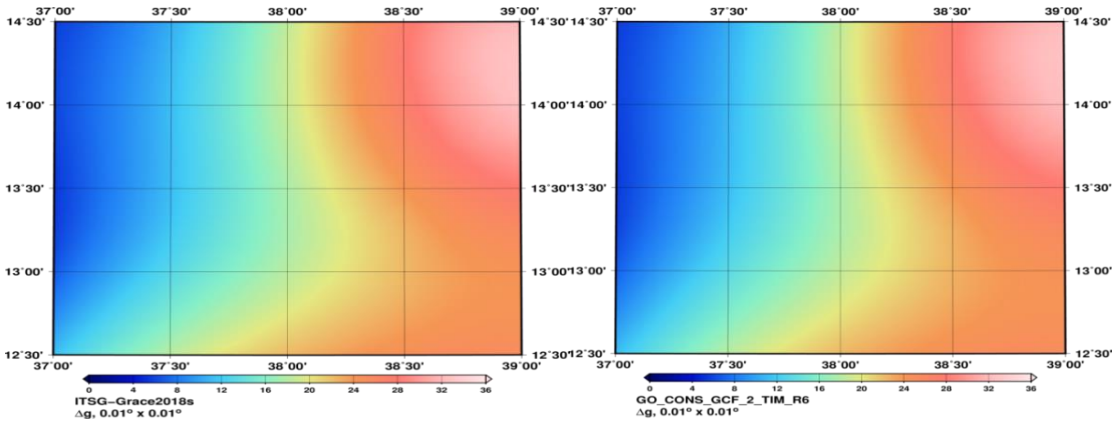

(a) (b)

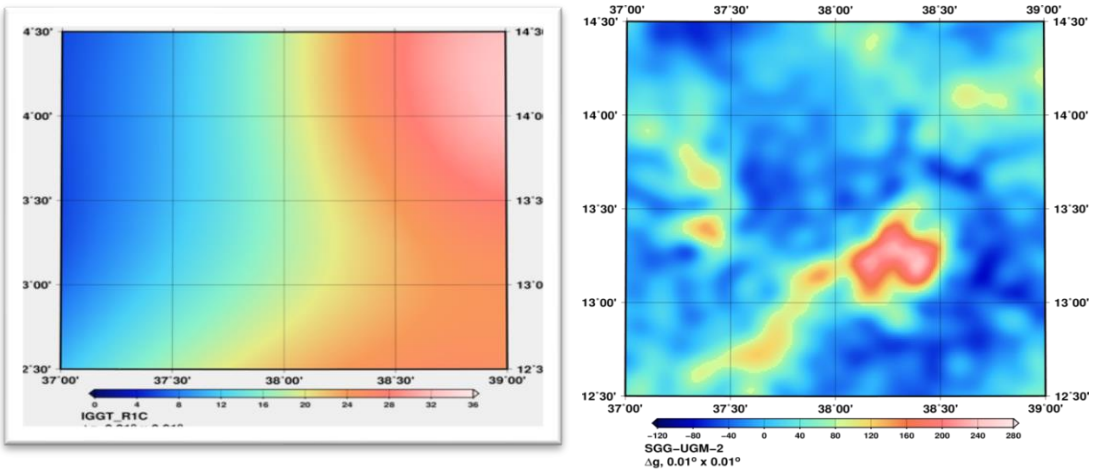

c) (d)

Figure 4.2 (a) gravity anomaly in model ITSG-G, (b) gravity anomaly in model GO_CON (c) gravity anomaly in model IGGT_R1C, (d) Ima gravity anomaly in model SGG-UG

The model IGGT_R1C shown in Figure 4.2 (c) is the result of the two satellite models, and in this model, the mean of the gravity anomalies is 7. 107mgal and the minimum and maximum gravity anomalies are 5.711 mgal and 32.560 mgal respectively. When we look at the model SGG-UGM-2, as shown in Figure 4.2 (d), we see that the range level is different from others, ranging from -120 to 280 mgal. The model shown in Figure 4.2 (d), SGG-UGM-2, is the result of the two satellite models and is made to a high degree of scale. In this model, the mean gravity anomaly is 14.194 mgal and the minimum and maximum gravity anomalies are -80.507 mgal and 242.900 mgal, respectively. As a summary, the four model results are shown in Table 4.2 below

Table 4.2 Summary of the gravity anomaly results of the four models.

Gravity model	ITSG-Grace2018s model(mgal)	IGGT_R1C GRACE Model(mgal)	GO_CONS_GCF_ 2_TIM_R6 Model (mgal)	SGG-UGM-2 Model(mgal)
min	5.441	5.711	4.901	-80.507
max	32.680	32.560	32.320	242.900
mean	7.064	7.107	7.129	14.194

The geoid height found in the four models with the same formula is found in the same range in the three models, which ranges from -3.08 meters to 00 meters. To compare the mean, minimum, and maximum, the ITSG-Grace2018s model shown in Figure 4.3 (a) is the only one made by the Gravity Recovery and Climate Experiment satellite, and in this model, the mean of

the geoid height is 0.618 meters, with the minimum and maximum geoid height being -3.037 meter and -0.041 meter, respectively. The model shown in Figure 4.3 (b) is GO_CONS_GCF_2_TIM_R6 GOCE, and only the Gravity Field and Stable State Ocean Circulation Explorer satellite is used. The mean of the geoid height using the GO_CONS_GCF_2_TIM_R6 GOCE data model is 0.614 meters, and the minimum and maximum geoid height are -3.037 meters and -0.398 meters respectively.

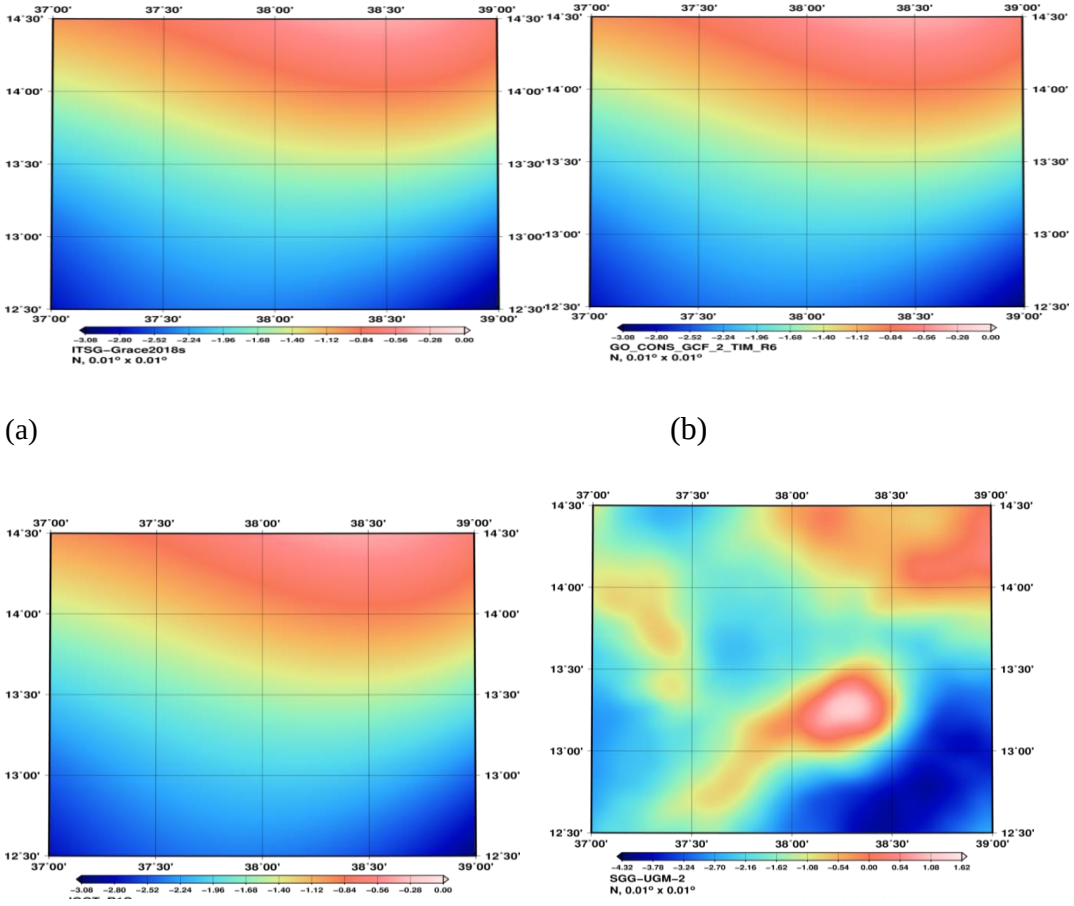

(a) (b)

© (d)

Figure 4.3. (a) Image of geoid height in model ITSG-G, (b) Image of geoid height in model GO_CON, © Image of geoid height in model IGGT_R1C, (d) Image of geoid height in model SGG-UGM-2

The model IGGT_R1C shown in Figure 4.3 (c) is the result of the two satellite models, and in this model, the mean of the geoid height is 0.614 meters and the minimum and maximum height anomaly is -3.037 meters and -0.398 meters respectively. When we look at the model SGG-UGM-2, as shown in Figure 4.3 (d), we see that the range level is different from others, ranging from -120 to 280 meters. The model shown in Figure 4.3 (d), SGG-UGM-2, is the result of the two satellite models and is made to a high degree of the scale. In this model, the mean height

anomaly is 1.225 meters, and the minimum and maximum height anomalies are -4.012 meters and -1.687 meters, respectively. A summary, the four model result is shown in Table 4.3 below

Table 4.3 Summary of the geoid height output of the four models

Gravity model	ITSG-Grace2018s (m)	IGGT_R1C GRACE(m)	GO_CONS_GCF_2_TIM_R6 (m)	SGG-UGM-2(m)
min	-3.037	-3.037	-3.037	-4.012
max	-0.041	-0.398	-0.398	1.225
mean	0.618	0.614	0.614	-1.687

The height anomaly found in the four models with the same formula is found in the same range in the three models, which range from 0 to 36 mgal. To compare the mean, minimum, and maximum, the ITSG-Grace2018s model shown in Figure 4.4 (a) is the only one made by the Gravity Recovery and Climate Experiment satellite, and in this model, the mean of the height anomaly is 0.582 meters, with the minimum and maximum height anomaly being -2.647 meter and -0.185 meter, respectively. The model shown in Figure 4.4 (b) is GO_CONS_GCF_2_TIM_R6 GOCE, and only the Gravity Field and Stable State Ocean Circulation Explorer satellite is used. The mean of the height anomaly using the GO_CONS_GCF_2_TIM_R6 GOCE data model is 0.578 meters, and the minimum and maximum height anomaly are -2.650 meters and -0.178 meters respectively.

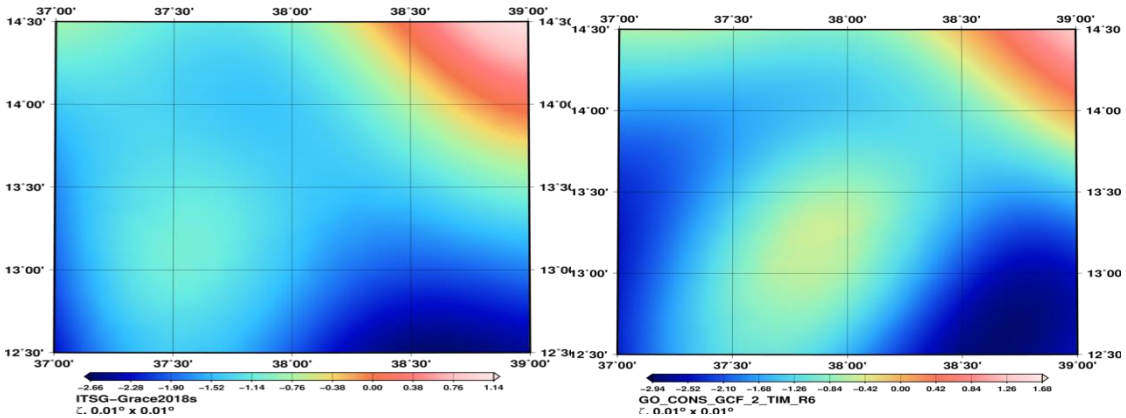

(a) (b)

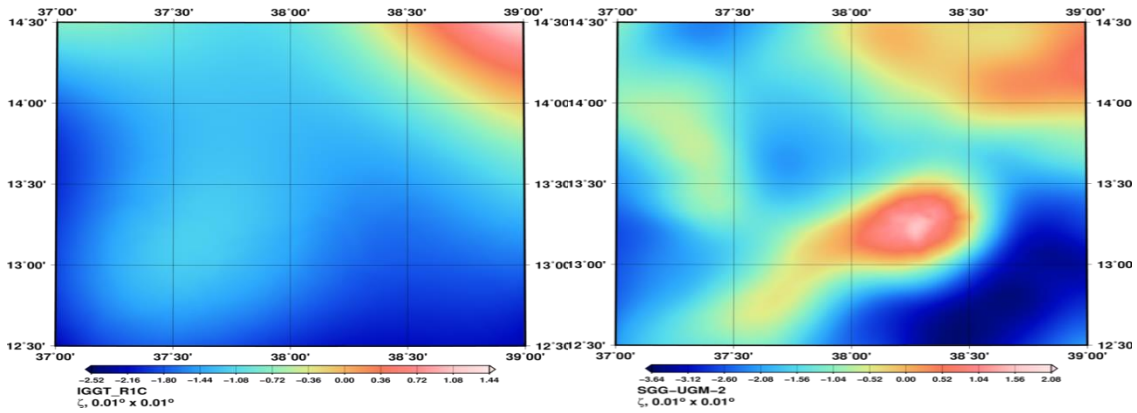

(c) (d)

Figure 4.4. (a) height anomaly in model ITSG-Grac2018s,(b) height anomaly in model GO_CONS ,(c) height anomaly in model IGG_R1C, (d) height anomaly in model SGG-UGM-2

The model IGGT_R1C shown in Figure 4.4 (c) is the result of the two satellite models, and in this model, the mean of the height anomaly is 0.576 meters and the minimum and maximum height anomaly is -2.647 meter and -0.196 meters respectively. When we look at the model SGG-UGM-2, as shown in Figure 4.4 (d), we see that the range level is different from others, ranging from -3.910 meters to 31.630 meters. The model shown in Figure 4.4 (d), SGG-UGM-2, is the result of the two satellite models and is made to a high degree of the scale. In this model, the mean height anomaly is 1.812 meters and the minimum and maximum height anomalies are -3.689 meters and -1.416 meters, respectively. A summary, the four-model result is shown in Table 4.3 below

Table 4.4 Summary of height anomaly results of the four models

Gravity model	ITSG Grace2018s model(m)	IGGT_R1C GRACE Model(m)	GO_CONS_GCF_2_TIM_R6 Model(m)	SGG-UGM-2 Model(m)
min	-2.650	-2.647	-2.650	-3.689
max	-0.185	-0.196	-0.178	1.812
mean	0.582	0.576	0.578	-1.416

Gravity Anomaly, Gravity Disturbance, Geoid and Quasi Geoid are processed for display from the available Gravity Fields, and since the 4041 cell is difficult to place, it is tried to describe some of them in the Appendix for display.

4.2 Computation of geoid-quasi-geoid separation from gravity model data

The geoid-quasi-geoid separation found in the four models with the same formula is within the same range in the three models. To compare the mean, minimum, and maximum, the ITSG-Grace2018s model shown in Figure 4.5 (a) is the only one made by the Gravity Recovery and Climate Experiment satellite, and in this model, the mean of the geoid to quasi-geoid separation is 0.604 meters, with the minimum and maximum geoid to quasi-geoid separation being 0.365 meters and 3.755 meters, respectively. The standard deviation for this model is 0.467meters. The model shown in Figure 4.5 (b) is GO_CONS_GCF_2_TIM_R6 GOCE, and only the Gravity Field and Stable State Ocean Circulation Explorer satellite is used. The mean of the geoid to quasi-geoid separation by using the GO_CONS_GCF_2_TIM_R6 GOCE data model is 0.605 meters, and the minimum and maximum geoid to quasi-geoid separation are 0.360 meters, and 3.760 meters, respectively.

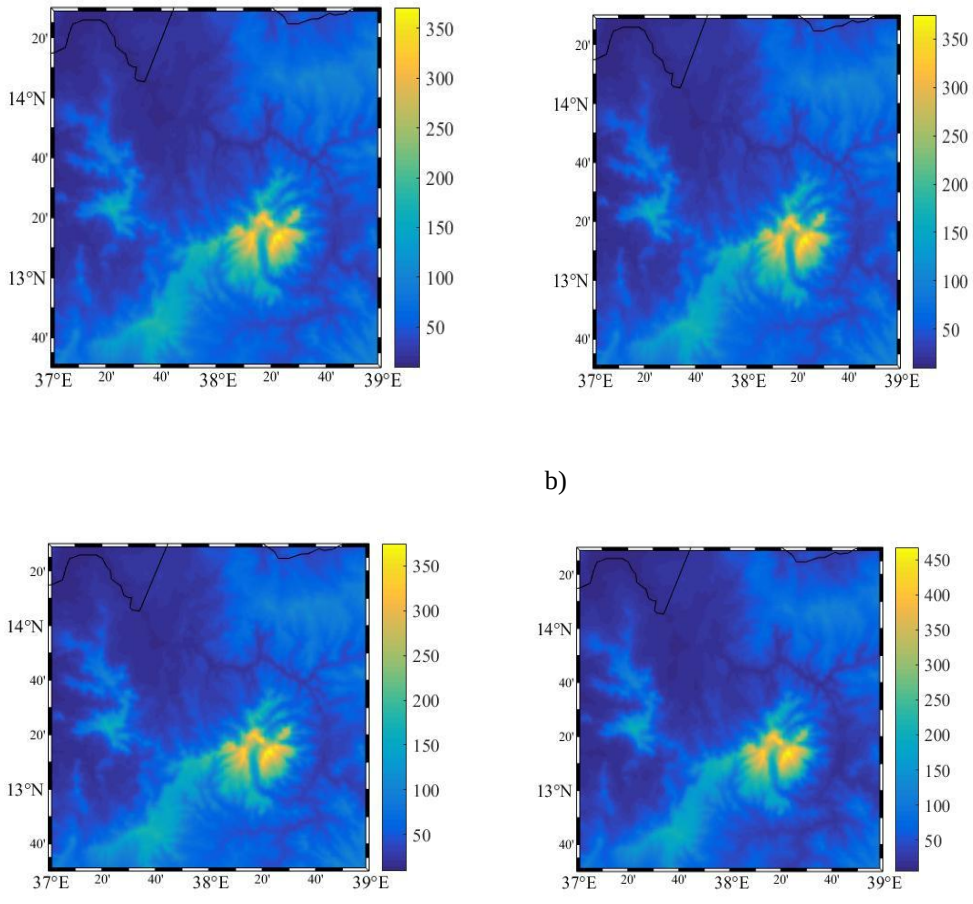

Figure 4.5 a) geoid quasi-geoid separation in model ITSG-Grace b) geoid quasi-geoid separation in model GO_CONS, © geoid quasi-geoid separation in model IGGT_R1C d) geoid quasi-geoid separation in model SGG-UGM-2

The standard deviation of the model is also 0.468.The model IGGT_R1C shown in Figure 4.5 (c) is the result of the two satellite models, and in this model, the mean of the geoid to quasi-geoid separation is 0.605 meter and the minimum and maximum geoid to quasi-geoid separation are 0.357 meters and 3.798 meters respectively. The standard deviation of the model is also 0.466. When we look at model SGG-UGM-2, as shown in Figure 4.5 (d), we see that the range level is different from others. The model shown in Figure 4.5 (d), SGG-UGM-2, is the result of the two satellite models and is made to a high degree of the scale. In this model, the mean geoid to quasi-geoid separation is 0.619 meter and the minimum and maximum geoid to quasi-geoid separation are 0.388 meters and 4.734 meters respectively. The standard deviation of the model is also 0.575. A summary, the four-model result is shown in table 4.5 below.

Table 4.5, summary of the geoid to quasi-geoid separation results of the four models.

Gravity model	ITSG-Grace2018s (m)	IGGT_R1C GRACE Model(m)	GO_CONS_GCF_2_TIM_R6 Model(m)	SGG-UGM-2 Model(m)
min	0.365	0.356	0.360	0.388
max	3.755	3.798	3.760	4.73
mean	0.604	0.605	0.605	0.619
s deviation	0.467	0.466	0.468	0.575

4.3 Comparison between different gravity field functions from gravity earth model result

When we look at Table 4.6, the results of the gravity field function between the three models, we see a close result, although there is some separation. According to this result, the lowest result obtained from each model was gravity disturbance, 4.825 mgal, 4.901 mgal, and 5.130 mgal, in that order. Even if we take an average, ITSG-Grace2018s, GO_CONS_GCF_2_TIM_R6, IGGT_R1C will get the same result of 7.123mgal, 7.129mgal, and 7.16mgal, respectively. Gravity anomaly, geoid, and height anomaly when we look at the Table4.5 gravity function between the three models; it shows almost the same result.

Table 4.6 Gravity function with three models

Name of model		gravity disturbance(mgal)	gravity anomaly(mgal)	Geoid(m)	height anomaly(m)	Type of model	Year	Reference
ITSG-Grace2018s	min	4.825	5.441	-3.037	-2.650	S(Grace)	2019	Mayer-Gürr, T. et al, 2018
	max	32.470	32.680	-0.041	-0.185			
	mean	7.123	7.064	0.619	0.582			
GO_CONS_GCF_2_TIM_R6	min	4.901	5.479	-3.037	-2.650	S(Goce)	2019	Brockmann, J. M. et al, 2021
	max	32.320	32.320	-0.399	-0.178			
	mean	7.129	7.073	0.614	0.578			
IGGT_R1C	min	5.130	5.711	-3.037	-2.647	G, S(Goce), S(Grace	2018	Lu, B. et al., 2019
	max	32.340	32.560	-0.398	-0.196			
	mean	7.160	7.107	0.614	0.576			

Unlike others, the difference set as a minimum on the geoid is -3.037 meters for all three. The negative result shows that the difference between the ellipsoid and the geoid is between the bottom and the top. It's a secret, but the distance (height) doesn't mean it's going to be negative. This gravity anomaly average is 7.064mgal in the Grace Model alone, 7.073mgal in the Goce Model alone, and 7.107mgal when we use the two data sets together, Grace and Goce. At least there is a slight difference in gravity field applications.

4.4 The effects of the number of degrees and order in the earth gravity model in the gravity field function computation.

In this section, we used the same data to look at what the gravity field functions look like at different degrees, and thus a very wide difference was observed. In this, we saw the IGGT_R1C model and SGG-UGM-2 with degrees of 240 and 2190 on the same grid number, respectively. disturbance, gravity anomaly, Geoid, and height anomaly If we look at the gravity field functions as display in Table 4.7, the smallest -81.486 mgal, -80.507 mgal, -4.012 meters, and-3.689 meters in the SGG-UGM-2 model are respectively, and their maximum amount is 243.159 mgal, 242.899 mgal, 1.225 meters, and-1.415 meters respectively.

Table 4:7 The Effects of Degree and Order in the Calculation of Gravity Field Functions

Name of model		gravity disturbance(mgal)	gravity anomaly(mgal)	Geoid(m)	height anomaly (m)	Type of model	degree	Reference
SGG-UGM-2	min	-81.486	-80.507	-4.012	-3.689	A, EGM2008, Grace), S (Goce)	2190	Liang, W. et al. 2020
	max	243.159	242.899	1.225	1.812			
	mean	13.759	14.194	-1.687	-1.416			
IGGT_R1C	min	5.130	5.711	-3.037	-2.647	G, S(Goce), S(Grace	240	Lu, B. et al., 2019
	max	32.340	32.560	-0.398	-0.196			
	mean	7.160	7.107	0.614	0.576			

On the other hand, the gravity field functions of the IGGT_R1C model are the lowest at 5.130 mgal, 5.711 mgal, -3.037 meters, -2.647 meters and the highest at 32.340 mgal, 32.560 mgal, -0.398 meters, -0.196 meters. It can be understood from Table 4.6 that there is a great difference between the two models when we use the same method.

CHAPTER FIVE

5. Discussion

This study's main goal is to compute gravity field functions using models created using satellite data, specifically with Gravity Recovery and Climate Experiment satellite data only, Gravity Field and Stable State Ocean Circulation Explorer satellite data only, to compute gravity field functions using the integrated data model, and to compute gravity field functions using each of these methods separately and compare them. An effort was made to investigate any potential variations. For this investigation, we employed the SGG-UGM-2, IGGT_R1C, ITSG-Grace2018s, and GO_CONS_GCF_2_TIM_R6 models that can be downloaded from the International Center Global Gravity Model. Additionally, E-topo was used for this research survey's height above sea level. The same area and formula are used for this work.

The Semien plateau study region, which is bordered by the parallels of 37 and 39 arc-degrees north latitude and the meridians of 12.5 and 14.5 arc-degrees east longitude, was the site of the numerical analysis. A 0.01 x 0.01 arc-degree geographic grid was used for all computations.The ITSG-Grace2018s, GO_CONS_GCF_2_TIM_R6, and IGGT_R1C coefficients were used to compute the gravity field variables with a spectral resolution complete to degree 200 of spherical harmonics. The gravitational field quantities were calculated using the SGG-UGM-2 coefficients at the same spectral resolution. The outcomes of the two models were contrasted.

One of the references that different writers have used to calculate the earth's height above sea level using gravitational field functions is the Geoid. The ellipsoid of a revolution, which is frequently used to simulate the form of the real Earth, is less irregular than the geoid surface, which is far smoother than the real Earth's surface. The determination of the geoid, which is described as an equipotential surface of the Earth's gravitational field that typically coincides with mean sea level, is one of the main objectives of geodesy. However, the Global Positioning System has been utilizing satellites to measure this height for centuries. An ellipsoid, not a geoid, was the original form of GPS. The primary responsibility of a geodesist is to understand their distinctions. Identifying the geoid's position in advance is one of the tasks that must be completed. The majority of geoid locations around the globe are underground, thus finding them will be difficult.

On the other hand, the Model sky theory, which is employed by another researcher, can address the issue of the unknown mass of the globe above mean sea level. Molodensky proclaimed the

geoid impossible to determine with sufficient accuracy and created an alternate quantity known as the quasi-geoid in the 1960s since the E topo density could not be determined with sufficient accuracy (and this issue still exists today). On Earth, there is also this potential energy. The result of this procedure is what is known as a Height Anomaly. Another name for the reference line is a quasi-geoid. The geoid quasi-geoid separation is the separation in space between the two hypotheses. The purpose of this study is to be able to find this difference using satellite data.

In actuality, we used the satellite data model to compute the gravitational field using the spherical formula from equations 14 to 30. As a consequence, the results shown below were attained. Saying this allowed us to identify the smallest to greatest numbers on the 40401 grid. In this manner, we comprehend the terrain's irregularity. The study's covered region has an average elevation of 4291.08 meters above sea level, with a minimum elevation of 653.8 meters. To examine the potential of various types of data, we have computed the same formula using various models. In this study, as can be seen, SGG-UGM-2, IGGT_R1C, ITSG-Grace2018s, and GO_CONS_GCF_2_TIM_R6 were calculated using the equation 14 to equation 30 formula, and the results showed that the lowest differences were 0.356656, 0.3648, and 0.360318257, while the highest results were 4.7341, 3.797842, 3.75480, and 3.75839724. The average outcomes for each grid were, as predicted, 0.61915, 0.604778, 0.60419, and 0.60461847. Between IGGT_R1C and ITSG-Grace2018s, there is a difference of 0.043042, and between ITSG-Grace2018s and GO_CONS_GCF_2_TIM_R6, there is a difference of 0.0049. This is a notable distinction. We have noticed the similar behavior when examining various gravity field functions. We should point out, though, that we combine the two in Gravity Recovery and Climate Experiment and Gravity Field and Stable State Ocean Circulation Explorer. We observe similarity to the same degree as a result. The size of the degrees, on the other hand, is what we perceive as the geodesic-wide difference. Gravity Recovery and Climate Experiment and Gravity Field and Gravity Field and Stable State Ocean Circulation Explorer satellite data were used to create the models SGG-UGM-2 and IGGT_R1C. The model with a higher degree has a noticeable difference from the others when we compare how they differ from one another.

CHAPTER 6

6. Conclusions And Recomendations

6.1 Conclusions

This study focused on the hills and the highest places in Ethiopia. This is exploring the difference between geoid and quasi-geoid using Earth models. For this survey, we used four models. The four models were selected based on the type of satellite used and the order size. Based on this, it uses three types of satellite data; those are only Gravity Recovery and Climate Experiment data, models made only by the Gravity Field and Stable State Ocean Circulation Explorer satellite, and models made using both satellite data. In addition to this, the degree used when making the models was also shown in the function of the gravity field.

In general, from the result, we were able to observe different gravity fields in all four types of models. In this, we observed the results of low to high-gravity fields. From the gravity fields that we surveyed in this study, they were observed from the result at the end of each model. The maximum size and the minimum size are also the average results. To see the geoid quasi-geoid that we started with, the largest difference was recorded by the SGG-UGM-2 model, and close results were recorded by the other three models.

From the analysis, the gravity fields were obtained by the four models, and the results obtained by the three models are close. The model with the highest degree has a different result. The difference is caused by the high degree and the large area covered. The difference between the Gravity Recovery and Climate Experiment and Gravity Field and Stable State Ocean Circulation Explorer satellite data model at a small spatial extent and at a small degree is not exaggerated.

6.2 Recommendations’

The result has not found many articles in this field, like in our country, Ethiopia, and to reach the civilization that the world has reached, it should be the homework of institutions to produce scholars who are educated in the field and who can conduct research. There should be an institution where models can be prepared. The use of earth models to calculate the gravity field in countries with difficult terrain like Ethiopia is useful for accessing difficult areas.

REFERENCES

Africa, E. (n.d.). *Animal Feed Action Plan*.

Ågren, J., Sjöberg, L. E., & Kiamehr, R. (2008). *Computation of a New Gravimetric Geoid Model over Sweden Using the KTH Method Computation of a New Gravimetric Geoid Model over Sweden Using the KTH Method*. *June*, 1–16.

Ah, Z., & Akhter, G. (2009). *A s tudy on the evaluation of the geoid-qua s igeoid s eparation term over Paki s tan with a s olution of fir s t and s econd order height term s*. *1995*, 815–823.

Al-Dabbagh, M. E. (2014). The Arabian Plate: unique fit of the earth's surface jig saw puzzle. *Arabian Journal of Geosciences*, *7*(8), 3297–3307. https://doi.org/10.1007/s12517-013-0979-1

Austin, P. A. (2016). African Volume Volume Copyright : In *Published by: African Wildlife Foundation: Vol. V*.

Bagherbandi, M., & Tenzer, R. (2013). *Geoid-to-Quasigeoid Separation Computed Using the GRACE / GOCE Global Geopotential Model GOCO02S - A Case Study of Himalayas and Tibet*. *24*(1), 59–68. https://doi.org/10.3319/TAO.2012.09.17.02(TT)1.

Barthelmes, F. (2013). *Definition of Functionals of the Geopotential and Their Calculation from Spherical Harmonic Models*. *January*. https://doi.org/10.2312/GFZ.b103-0902-26

Chanard, K., Avouac, J. P., Ramillien, G., & Genrich, J. (2014). *Journal of Geophysical Research : Solid Earth Modeling deformation induced by seasonal variations of continental water in the Himalaya region :* 5097–5113. https://doi.org/10.1002/2013JB010451.Abstract

Chernet, T. (2015). *A Resource Base and Climate Change Risk Maps for Simien Mountains National Park*.

Eshagh, M. (2017). Local recovery of lithospheric stress tensor from GOCE gravitational tensor. *Geophysical Journal International*, *209*(1), 317–333. https://doi.org/10.1093/gji/ggx026

Gedamu, A. A., Eshagh, M., & Bedada, T. B. (2020). Moho determination from GOCE gradiometry data over Ethiopia. *Journal of African Earth Sciences*, *163*. https://doi.org/10.1016/j.jafrearsci.2019.103741

Gile, P. P., Buljac-samardzic, M., & Klundert, J. Van De. (2018). *The effect of human resource*

management on performance in hospitals in Sub-Saharan Africa : a systematic literature review. 1–21.

Hofmann-Wellenhof, B., & Moritz, H. (2005). Physical geodesy. In *Physical Geodesy*. Aalto University. https://doi.org/10.1007/b139113

Hofmann, Moritz, B., Flury, J., Rummel, R., Foroughi1, I., Tenzer, R., & Sjöberg, L. E. (2017). Helmut Moritz Physical Geodesy SpringerWienNewYork. In *Journal of Geodesy* (Vol. 84, Issue 9).

Huang, J., & Véronneau, M. (2013). *Canadian gravimetric geoid model 2010*. https://doi.org/10.1007/s00190-013-0645-0

Jekeli, C., Jin, H., & Jay, Y. (2009). *Using gravity and topography-implied anomalies to assess data requirements for precise geoid computation*. 1193–1202. https://doi.org/10.1007/s00190-009-0337-y

Journal, T. *A. (2008). The Density Probability Distribution In Compressible Isothermal Turbulence: Solenoidal Versus Compressive Forcing Christoph Federrath, 1,2 Ralf S. Klessen, 1 and Wolfram Schmidt 3*. 2006–2009.

Kingdon, R., Santos, M., & Van, P. (2012). *physics versus geometry*. *42*, 101–117.

Klinger, B., & Mayer-gürr, T. (n.d.). *ITSG-Grace2016 data preprocessing methodologies revisited : impact of using Level-1A data products*. 2016. https://doi.org/10.5880/icgem.2016.007

Kvas, A., Brockmann, J. M., Krauss, S., Schubert, T., Gruber, T., Meyer, U., Mayer-gürr, T., Schuh, W., Jäggi, A., & Pail, R. (2021). *GOCO06s – a satellite-only global gravity field model*. *002*(June 2020), 99–118.

Liang, W., Li, J., Xu, X., Zhang, S., & Zhao, Y. (2020). A High-Resolution Earth's Gravity Field Model SGG-UGM-2 from GOCE, GRACE, Satellite Altimetry, and EGM2008. *Engineering*, *6*(8), 860–878. https://doi.org/10.1016/j.eng.2020.05.008

Lu, B., Luo, Z., Zhong, B., Zhou, H., Flechtner, F., Förste, C., Barthelmes, F., & Zhou, R. (2018). The gravity field model IGGT_R1 based on the second invariant of the GOCE gravitational gradient tensor. *Journal of Geodesy*, *92*(5), 561–572. https://doi.org/10.1007/s00190-017-1089-8

Mayer-Gürr, T., Behzadpur, S., Ellmer, M., Kvas, A., Klinger, B., Strasser, S., & Zehentner, N. (2018). ITSG-Grace2018 - Monthly, Daily and Static Gravity Field Solutions from GRACE. In *GFZ Data Services*.

Mccubbine, J. C., & Featherstone, W. E. (2018). Error propagation for the Molodensky G 1 term. *Journal of Geodesy*, *2017*. https://doi.org/10.1007/s00190-018-1211-6

Mehramuz, M., & Zomorrodian, H. (2013). *Study of geoid – quasigeoid separation obtained from terrestrial gravity data and two geopotential models*. https://doi.org/10.1007/s12517-013-1014-2

Molnar, P., England, P. C., & Jones, C. H. (2015). Mantle dynamics, isostasy, and the support of high terrain. *Journal of Geophysical Research: Solid Earth*, *120*(3), 1932–1957. https://doi.org/https://doi.org/10.1002/2014JB011724

Moritz, H. (1992). *G*eodetic Reference System 1980. 128–162.

Pellinen, L. P. (1972). Physical Geodesy. *Bulletin Géodésique*, *46*(2), 133–138. https://doi.org/10.1007/BF02530297

Plan, M. (2015). *The Federal Democratic Republic Of Ethiopia Sustainable Tourism*.

Poutanen, M. (2020). *Geodesy The Handbook* (Vol. 94, Issue 11).

Sadiq, M., Ahmad, Z., & Akhter, G. (2009). *A study on the evaluation of the geoid-quasigeoid separation term over Pakistan with a solution of first and second order height terms*. *1995*, 815–823.

Schubert, G., Turcotte, D. L., & Olson, P. (2001). *Mantle Convection in the Earth and Planets*. Cambridge University Press. https://doi.org/DOI: 10.1017/CBO9780511612879

Seid, A. (2019). No Title. *Validation of EGM - 08 Using GPS and LEVELING in Addis Ababa*, *June*.

Shandini, Y., & Tadjou, J. M. (2012). *Interpreting gravity anomalies in south Cameroon , central Africa*. *16*(1), 5–9.

Sjo, L. E. (2000). *Topographic e € ects by the Stokes ± Helmert method of geoid and quasi-geoid determinations*. 255–268.

Sjöberg, L. E. (2008). *Answers to the comments by M . Vermeer on L . E . Sjöberg (2007) " The*

topographic bias by analytical continuation in physical geodesy " J Geod 81 : 345 – 350. 451–452. https://doi.org/10.1007/s00190-007-0193-6

Sjöberg, L. E. (2010). *Short Note A strict formula for geoid-to-quasigeoid separation*. 699–702. https://doi.org/10.1007/s00190-010-0407-1

Sjöberg, L. E. (2018). *On the geoid and orthometric height vs . quasigeoid and normal height*. 115–120.

Tassis, G. A., Grigoriadis, V. N., Tziavos, I. N., Tsokas, G. N., & Papazachos, C. B. (2013). *A new Bouguer gravity anomaly field for the Adriatic Sea and its application for the study of the crustal and upper mantle structure*. *66*, 38–52.

Tenzer, R., Moore, P., & Kuhn, M. (2006). *Explicit formula for the geoid-quasigeoid separation*. *January*. https://doi.org/10.1007/s11200-006-0038-4

Tenzer, R., Novák, P., Moore, P., Kuhn, M., & Vaníček, P. (2006). Explicit formula for the geoid-quasigeoid separation. *Studia Geophysica et Geodaetica*, *50*(4), 607–618. https://doi.org/10.1007/s11200-006-0038-4

Toth, G., & Torge, W. (2008). *Geodesy. Lecture Notes*. *2*.

Vaníček, P. (1976). *Physical Geodesy* (Issue 43).

Xu, X., Zhao, Y., Reubelt, T., & Tenzer, R. (2017). Geodesy and Geodynamics A GOCE only gravity model GOSG01S and the validation of GOCE related satellite gravity models. *Geodesy and Geodynamics*, *8*(4), 260–272. https://doi.org/10.1016/j.geog.2017.03.013

Appindex

NO.	longitude [deg.]	latitude [deg.]	h_over_geoid [meter]	height_anomaly [meter]	gravity_anomaly_sa [mgal]	gravity_disturbance-sa [mgal]	geoid [meter]	gravity_anomaly [mgal]
25666	38.38	13.23	4291.08	1.0226	359.5319	360.3306	0.7879	234.9308
25465	38.38	13.24	4274.6	1.0562	352.4733	353.2710	0.8129	233.5188
25665	38.37	13.23	4264.32	1.1150	345.4905	346.2958	0.8650	233.1188
26065	38.35	13.21	4257.8	1.1829	304.9243	305.6954	0.9006	220.3491
25864	38.35	13.22	4239.2	1.2351	306.6662	307.4539	0.9502	223.0928
26266	38.35	13.2	4235	1.1319	302.5020	303.2521	0.8397	217.3992
25464	38.37	13.24	4229.6	1.1535	340.0473	340.8534	0.8910	232.5804
25667	38.39	13.23	4210.32	0.9650	368.8224	369.6065	0.7015	237.2055
25664	38.36	13.23	4208.36	1.2103	327.7642	328.5692	0.9320	230.2321
25264	38.38	13.25	4203.2	1.0987	342.6363	343.4261	0.8296	231.6882
25867	38.38	13.22	4197.72	1.0194	363.9845	364.7775	0.7538	237.2605
25466	38.39	13.24	4181.6	1.0030	360.9674	361.7495	0.7253	235.7080
24254	38.33	13.3	4178.4	1.2910	284.3575	285.1273	1.0856	211.0550
25067	38.42	13.26	4176.52	0.7335	333.8361	334.4993	0.4311	215.9077
25865	38.36	13.22	4156.04	1.1919	329.2388	330.0347	0.8950	230.4813
25868	38.39	13.22	4151.28	0.9499	373.6781	374.4571	0.6691	239.1082
25663	38.35	13.23	4137.8	1.3012	307.6137	308.4132	0.9886	226.2662
25866	38.37	13.22	4124.88	1.1275	348.8003	349.5985	0.8293	235.8474
26066	38.36	13.21	4124.36	1.1550	329.3175	330.0989	0.8472	229.2488
24253	38.32	13.3	4122.6	1.3269	294.8528	295.6422	1.1146	215.2753
24866	38.42	13.27	4118.6	0.7515	317.3040	317.9453	0.4301	210.2622
25265	38.39	13.25	4109	1.0462	349.9761	350.7491	0.7412	233.4792
25263	38.37	13.25	4107.8	1.2105	332.2500	333.0505	0.9081	232.2761
25066	38.41	13.26	4107.08	0.8625	338.3145	339.0158	0.5449	222.5785
25463	38.36	13.24	4106.84	1.2685	324.6856	325.4940	0.9589	231.6083
26267	38.36	13.2	4103	1.1030	328.0994	328.8610	0.7883	226.7538
25248	38.22	13.25	4093.8	1.4091	289.8788	290.6843	1.1362	212.3302
26467	38.35	13.19	4085	1.1084	299.3587	300.0833	0.7675	215.6460
26466	38.34	13.19	4083.8	1.1728	270.4727	271.1798	0.8064	207.0413
25448	38.21	13.24	4082.48	1.3803	297.2260	298.0311	1.0948	213.2642
25649	38.21	13.23	4078.84	1.3838	293.1354	293.9360	1.0816	212.0921

26667	38.34	13.18	4076.8	1.0948	266.0522	266.7292	0.7218	201.9391
25668	38.4	13.23	4075.8	0.9236	372.5569	373.3175	0.6066	238.7193
25449	38.22	13.24	4075.32	1.4262	284.1562	284.9580	1.1287	211.2748
26265	38.34	13.2	4071.8	1.2453	274.5935	275.3271	0.8805	211.7397
23445	38.28	13.34	4071.2	1.0686	323.6282	324.3702	0.9632	208.6345
23849	38.3	13.32	4070.2	1.2354	316.5302	317.3143	1.0737	215.7940
25247	38.21	13.25	4070	1.3722	298.5360	299.3391	1.0982	213.2838
23646	38.28	13.33	4064.52	1.1492	329.7272	330.5011	1.0218	214.6538
25650	38.22	13.23	4061.88	1.4316	276.2817	277.0739	1.1107	208.8950
25268	38.42	13.25	4060	0.7674	346.8102	347.4881	0.4254	223.5282
25851	38.22	13.22	4058.52	1.4237	266.7077	267.4850	1.0819	205.2849
25068	38.43	13.26	4056.28	0.6630	325.0435	325.6612	0.3111	211.2843
23645	38.27	13.33	4048.68	1.1402	329.2257	329.9945	1.0117	213.5801
24865	38.41	13.27	4047.48	0.8803	320.5538	321.2317	0.5448	216.5165
23647	38.29	13.33	4046.2	1.1661	323.8605	324.6302	1.0268	214.1342
25869	38.4	13.22	4045.2	0.8990	377.0885	377.8437	0.5762	240.0485
25063	38.38	13.26	4043.96	1.1594	329.8740	330.6491	0.8384	229.8943
25850	38.21	13.22	4042.96	1.3871	286.6264	287.4164	1.0583	210.1117
24052	38.32	13.31	4041.72	1.2971	291.8096	292.5784	1.0838	212.4656
26666	38.33	13.18	4041.04	1.1620	235.7903	236.4465	0.7491	193.0019
26867	38.33	13.17	4037.56	1.0739	230.6560	231.2783	0.6541	187.1264
24053	38.33	13.31	4036.68	1.2811	277.2320	277.9770	1.0555	207.7545
26068	38.38	13.21	4036.52	1.0314	365.9861	366.7669	0.7098	239.7873
26067	38.37	13.21	4035.68	1.1113	350.1524	350.9375	0.7834	236.3592